DEGREE PROJECT

Modelling of the thermal environment and subsystem for a 6U cubesat in GTO orbit

Vidhyuth Kasturi Chakravarthy Iyengar

Space Engineering, master's level (120 credits)
2022

Luleå University of Technology
Department of Computer Science, Electrical and Space Engineering

LULEÅ UNIVERSITY OF TECHNOLOGY

Modelling of the thermal environment and subsystem for a 6U cubesat in GTO orbit

Vidhyuth Kasturi Chakravarthy Iyengar

School of Science

Thesis submitted for examination for the degree of Master of Science in Technology.

Espoo 16.1.2021

Thesis supervisor:

Prof. Johnny Ejemalm

Thesis advisor:

Prof. Jaan Praks

Aalto University
School of Science

LULEÅ UNIVERSITY OF TECHNOLOGY

AALTO UNIVERSITY
SCHOOL OF SCIENCE

ABSTRACT OF THE
MASTER'S THESIS

Author: Vidhyuth Kasturi Chakravarthy Iyengar

Title: Modelling of the thermal environment and subsystem for a 6U cubesat in GTO orbit

Date: 16.1.2021 Language: English Number of pages: 7+62

Department of Electrical Engineering

Professorship: Nano-Satellites

Supervisor: Prof. Johnny Ejemalm

Advisor: Prof. Jaan Praks

The thermal design of the spacecraft ensures the unobstructed and smooth operation of the spacecraft under the harsh space conditions. As small satellites are getting more accessible and standardized, their uses are growing more into mission scenarios which are conventionally used by larger satellites. High altitude orbits are generally used by satellites which will need higher ground coverage, Deep space observations,and missions that want to study the radiation belts around the Earth.

In this thesis we study the impact of the space environment on a 6U CubeSat in a Highly Elliptical Orbit (HEO) around Earth. The Black Body loading and temperature graphs of the spacecraft in various orbital seasons, the impact of loading due to major heat sources and its variation with orbit perturbations, the impact of orbital inclination and satellite rotation on the loading of the satellite are studied.The orbital loading simulations are performed in NX space systems thermal solver to study the loading profile on the spacecraft model, based on which further studies are performed to find possible solutions that can be applicable for the solution. Foresail-2 mission design is considered for the loading simulation in orbit with Foresail-1 mission as the heritage mission. The thermal solutions hence applicable for consideration are presented.

Keywords: Cubesat, Thermal Design, Space Systems, Space Thermal Environment

Preface

I want to thank Professor Jaan Praks and Muhammad Mughal Rizwan for their precise instructions and diligent guidance Without which I will have not been able to complete my work. I will also like to thank Aalto University and Luleå University of technology for the opportunity to write this thesis.

Contents

Abstract ii

Preface iii

Contents iv

Symbols and abbreviations vi

1 Introduction 1
- 1.1 Trends in Small-satellite launches . . . 1
- 1.2 Foresail Missions . . . 3
  - 1.2.1 Foresail-1 . . . 3
  - 1.2.2 Foresail-2 . . . 4
- 1.3 CubeSat Thermal Design . . . 5
- 1.4 Problem Definition: Thermal Environment modelling . . . 6

2 Spacecraft Thermal Design Principles 7
- 2.1 Heat Transfer Principles . . . 7
  - 2.1.1 Conduction . . . 7
  - 2.1.2 Radiation . . . 8
  - 2.1.3 Steady State Heat Transfer . . . 9
- 2.2 Thermal Environment Of Geocentric Orbit . . . 11
  - 2.2.1 Direct Solar Radiation . . . 11
  - 2.2.2 Earth Albedo Radiation . . . 12
  - 2.2.3 Earth IR Radiation . . . 12
- 2.3 Thermal Design Principles . . . 13
  - 2.3.1 Spacecraft Heat Balance Equation . . . 13
- 2.4 Heritage Missions . . . 14

3 Geocentric Orbit Thermal Environment 15
- 3.1 Black Body Analysis . . . 15
- 3.2 Spacecraft Loading . . . 22
  - 3.2.1 Incident Solar Loading . . . 22
  - 3.2.2 Earth Albedo Loading . . . 24
  - 3.2.3 Earth IR Loading . . . 25
  - 3.2.4 Seasonal Loading . . . 26
- 3.3 Inclination Of The Spacecraft Orbit . . . 29
- 3.4 Loading On A Rotating Satellite . . . 32

4 Foresail-2 Design Overview 33

5 Spacecraft Thermal Design Consideration 34
- 5.1 Surface Coatings For GTO . . . 34
- 5.2 Solar Panel Modelling . . . 42
- 5.3 Spacecraft Internal Power . . . 46

5.4 Thermal Simulation Of Spacecraft 48
5.5 Spacecraft Heat Transfer Model 50
5.6 Surface Degradation 52

6 Conclusion **53**

References **55**

A Spacecraft Rotation **58**

Symbols and abbreviations

Latin Symbols

k	Thermal Conductivity (material specific)
A	Surface Area
T	Temperature of Lattice
t	Time
x	Specified Distance
E_{abs}	Absorbed Energy
E_{emit}	Emitted Energy
Q_{in}	Power Flowing Into The System
Q_{out}	Power Flowing Out Of The System
E_{wall}	Energy At The Wall Of The System
$Q_{cond,wall}$	Power Conducted Through The Wall
L	Length Of The Wall
R_{wall}	Resistance To Heat Flow Through The Wall
Q_{rad}	Power Radiated To/From The System
R_{rad}	Resistance To Radiation Heat Transfer
Q_{solar}	Power Absorbed From Incident Solar Radiation
G_{solar}	Incident Solar Radiation
T_o	Wall Outside Temperature
T_L	Temperature Of The Wall At Distance L
A_{inc}	Area Of The Surface Facing The Sun
Q_{albedo}	Power Absorbed From Earth Albedo
A_{plate}	Area Of Plate Facing Earth
a	Percentage Of Radiation Reflected From Earth (depends on the surface cover of Earth)
K_a	Earth View Factor
q_1	Earth IR Radiation At Surface Level
G	IR Radiation From Earth At Spacecraft Altitude Level
$Q_{internal}$	Internal Power Generated By The System

Greek Symbols

α	Thermal Absorptivity (material specific)
ϵ	Thermal Emissivity (dependent on material and temperature)
σ	Stefan Boltzmann Constant $\approx 5.67E-8W.m^{-2}.K^{-4}$
θ	Angle Between The Incident Sun Vector And The Affected Plate Surface Normal
β	Angle Between The Orbit Plane And The Sun Vector
ρ	Half Angle Of The Spacecraft Solid Angle Of The Earth View

Abbreviations

LEO	Low Earth Orbit
GTO	Geostationary Transfer Orbit
HEO	Highly Elliptical Orbit
GEO	Geosynchronous Equatorial Orbit
ULF	Ultra Low Frequency
CAD	Computer Aided Design
ACRIMSAT	Active Cavity Radiometer Ir-radiance Monitor Satellite
IR	Infrared
UV	Ultraviolet
VUV	Vacuum Ultraviolet
MLI	Multi Layer Insulation
NASA	National Aeronautics and Space Administration
PATE	Particle Telescope
REPE	Relativistic Electron and Proton Experiment
PB	Plasma Brake
MarCO	Mars Cube One
RAAN	Right ascension of the ascending node
RPM	Rotations Per Minute
TTC	Tracking, Telemetry and Control
PCB	Printed Circuit Board
ADCS	Attitude Determination and Control System

1 Introduction

The spacecraft is subject to space environmental conditions which cause extreme heating or cooling of the spacecraft. The loading on the spacecraft depends on spacecraft surface properties and the orbital conditions the spacecraft will be operating in, and the internal heat generated by the satellite. High-temperature variation or high thermal loads is detrimental to the spacecraft subsystem operations and can lead to critical failures in the spacecraft operations. The gradient between the sun-lit part of the satellite to the side in shadow can be high. Most of the subsystems have optimal operational temperatures that need to be maintained for reliable operation. Hence design considerations must be made to combat the extremes of the space thermal environment and its impact on a specific mission and ensure that the spacecraft is operating under the temperature ranges as per guidelines.

1.1 Trends in Small-satellite launches

Small Satellites	**Wet Mass**
pico-sat	$\leq$ 1 Kg
nano-sat	1 - 10 Kg
Micro-sat	11 - 100 Kg
Mini-sat	101 - 500 Kg

Table 1: Classification of Small satellites according to their wet mass

The number of CubeSat launches jumped from 24 in 2012 to 81 in 2013 as well as scientific experiments doubled in number. Due to the availability of compact technologies and the standardisation of design of CubeSats and cheaper manufacturing costs, the prospect of CubeSat applications for commercial as well as scientific experiments has increased exponentially [6].

The commercialisation of nano-satellites as cheaper alternatives to conventional satellite designs opens the avenue of nanosat launches for missions involving higher, more extreme orbits than the conventional LEO which has been dominated by nanosats [7]. While extensive CubeSat missions have embarked to orbits classified as LEO, missions to GTO have been few.

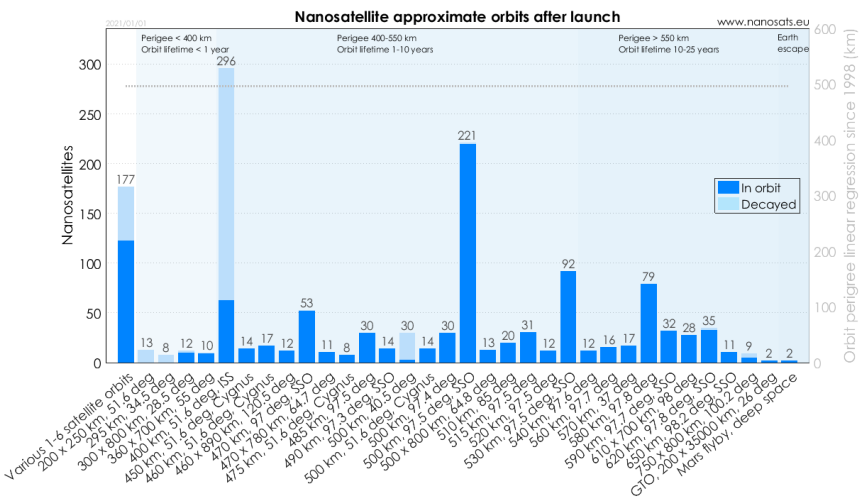

Figure 1: number of nanosats according to the orbit altitude [7]

Low Earth Orbit (LEO) is a type of Earth-centered orbit with low eccentricity and altitudes below 2000 km. These orbits are generally characterized by an eccentricity less than 0.25 and an orbital period of fewer than 128 minutes. Most of the artificial satellites in space are in LEO orbit [27]. LEO environment is generally under the influence of major heat sources and has lower cool eclipse periods as the satellite orbital period is comparatively higher [21]. Thermal design for a spacecraft to LEO has extensive heritage data and the study into the environment interaction has been studied.

Geostationary transfer orbit (GTO) is a type of highly elliptical orbit (HEO) with low inclination, the apogee of which ranges till 42000 km and the perigee of a few hundred kilometers above sea level. Its perigee altitude corresponds to the orbital height of LEO white its apogee altitude corresponds to that of the Geostationary orbit [1] [2]. HEOs are primarily used as orbits for communications satellites and observation satellites. In HEO, the motion of the satellite to and from the apogee is slow and hence will be over the corresponding region on the surface for a longer duration [3].

The Mars Cube One (MarCO) satellite was a CubeSat mission to Mars along with the InSight Mars lander mission by NASA. MarCO satellites were used as communication conduits for the InSight Mars lander to be able to communicate with observers on Earth. The successful use of MarCO satellites has emboldened CubeSat missions to have mission operations out of LEO [12]. GTO has been the focus of missions such as GTOSat by NASA, to study the Van Allen belt. Hence it is of great importance to study the possible implications of the changes in the environment between LEO and GTO concerning the thermal loading of the spacecraft. Due to the lack of missions and their subsequent data regarding spacecraft thermal performance in GTO, it becomes important to make studies into what can be expected from spacecraft operations in this orbit.

1.2 Foresail Missions

The Foresail missions are two satellites named Foresail-1 and Foresail-2 designed and manufactured by Aalto University, Finland. Aalto University has successfully launched the Aalto-1 satellite in 2017 hosting payloads from the VTT technical research center of Finland, the University of Helsinki and Turku, and the Finnish Meteorological institute [8]. The Foresail-2 mission is planned to be launched to GTO while the Foresail-1 mission is being designed for LEO operation.

1.2.1 Foresail-1

Foresail-1 is a Nanosat mission from the Finish Centre of Excellence for Sustainable Space, designed and assembled by Aalto University, Finland. The foresail-1 mission includes two payloads, the Particle Telescope (PATE) from the University of Turku and a Plasma break experiment from the Finish Meteorological Institute. The mission is slated to be launched by late 2021 into LEO to measure radiation belt losses [9].

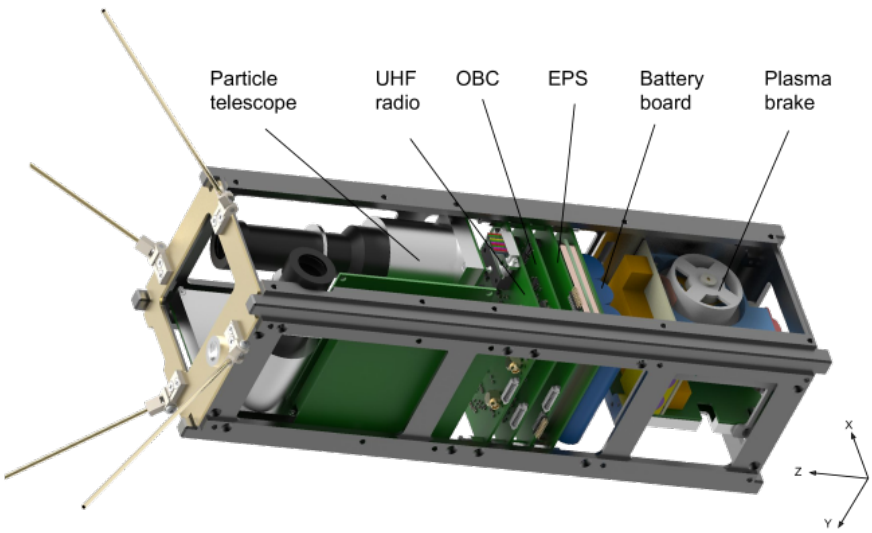

Figure 2: Foresail-1 Satellite model with subsystems [9]

PATE, the primary payload of the Foresail-1 mission, functions as a particle detector capable of measuring electrons and protons and their pitch angles and their energies. The secondary payload is the Electrostatic plasma brake developed by the Finnish Meteorological Institute as a proof of concept. The plasma break will be used to deorbit the satellite [9]. The Plasma brake experiment uses the friction between charged particles from solar winds and positively or negatively charged electric field around a tether to deorbit the satellite [11].

1.2.2 Foresail-2

Foresail-2 is the follow-up to the foresail-1 mission from the Finnish Centre of Excellence for Sustainable space designed and fabricated in Aalto University, Finland. Foresail-2 is designed as a 6U CubeSat carrying three payloads. The payloads include Relativistic Electron and Proton Experiment (REPE) telescope, Magnetometer and the Plasma brake experiment, heritage from the Foresail-1 experiment [13].

The foresail-2 mission will study the role of ULF waves in the acceleration, transportation, and scattering of electrons in the radiation belt as a function of solar wind along with the observation of the method of transportation of ULF waves and turbulence within the inner magnetosphere. Further, the plasma brake experiment will study how the Coulomb drag force will depend on the plasma parameters and tether voltage. The Coulomb drag will cause the satellite to deorbit [13].

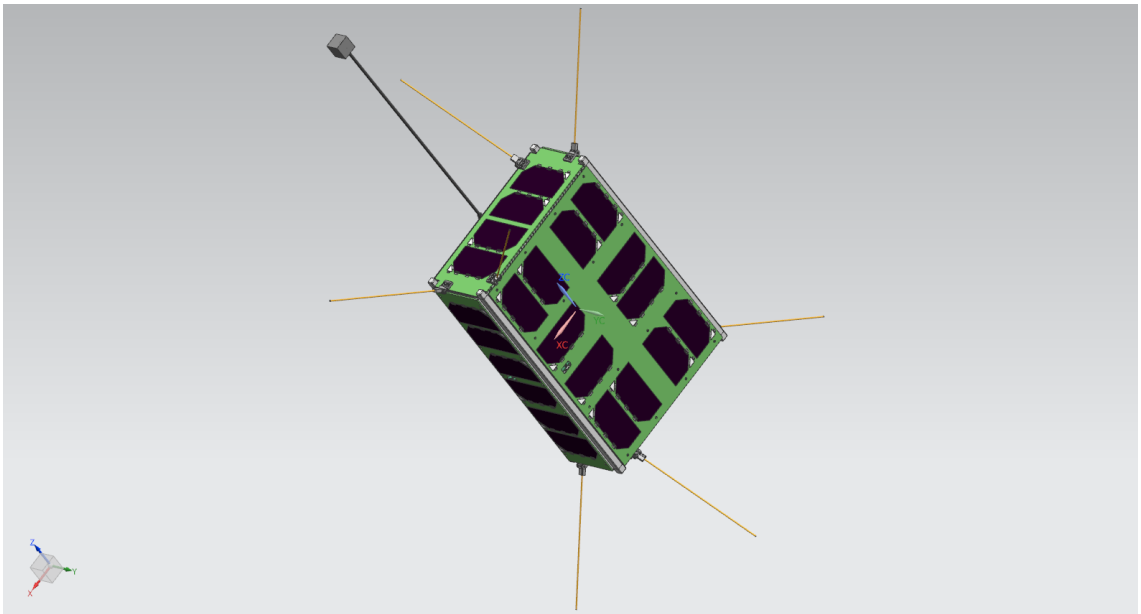

Figure 3: CAD model of the proposed 6U Foresail-2 satellite with Magnetometer boom extended [13]

The proposed model of the spacecraft can be observed in Figure 3. It is to be noted that the Foresail-2 mission is still in the design phase at the time this study was penned and hence many design changes could be expected in the final design of the spacecraft.

1.3 CubeSat Thermal Design

Spacecraft thermal solutions are generally classified as active and passive solutions. Passive heat transfer methods employ the use of heat transfer modes and vectors that do not require power for their operation. Active heat transfer solutions use forced heat transfer methods by introducing external force to achieve the heat transfer goal. Active heat transfer methods require more power and are costlier as compared to passive methods but are also more reliable and provide the designer with more versatility. Passive heat transfer solutions include Surface treatments and coatings, radiators, MLI, mirrors and reflectors, heat filters, etc. Active solutions include heaters, thermoelectric coolers, louvres, and fluid loops [17].

Satellite design engineers aim to solve the thermal loading on the satellite using passive solutions owing to their lower impact on the power budget of the spacecraft and also the comparatively lower cost coatings being the cheapest. MLI is the most commonly used passive thermal control method used to control spacecraft heating. Active thermal control methods provide the design with more flexibility to exert control over the thermal loading of the spacecraft and also provide more targeted capabilities in solving loading problems on specific subsystems.

Mission	**dimensions**	**Thermal Solution**	**Launch Date**
MarCO	6U	Insulation, Radiators and heaters	May 2018
GTOSat	6U	Thermal Louvres	2021
mDot	6U	Thermal Insulation and surface coatings	2021
SpectroCube	3U	N/A	2021
Orbital Factory II	1U	Surface finish	2021
LACCE	3U	N/A	N/A
ADE	1U	None	N/A
M-BARC/DSM-BRAC	3U	N/A	Cancelled
Shields-1	3U	Shielding Vaults	December 2019
BIRDY-GTO	3U	N/A	cancelled
ALCEK	6U	N/A	cancelled

Table 2: Missions to GTO and deep space since 2018 [25] [7]

1.4 Problem Definition: Thermal Environment modelling

The thermal design of a spacecraft depends on the environment that the spacecraft will be operating. The spacecraft's operational environment dictates the loading on the spacecraft. The design engineer will then solve the thermal loading problem on the satellite by adding necessary heat transfer manipulations. The thermal design process is iterative i.e. The thermal design process will require going through multiple solutions so that the most optimal one can be selected. The space environment not only affects the loading on the spacecraft but also causes the degradation of the spacecraft surfaces exposed to the space environment causing changes in the thermo-optical properties of the spacecraft surface [14]. Spacecraft thermal solutions for small satellites generally rely on controlling the thermo-optic properties of the spacecraft surface which is exposed to the space environment. As the dominant mode of heat transfer in space is radiation the loading on the spacecraft can be controlled using Paints, coatings, and surface finishes. Small satellites have limited space for power systems and hence have a smaller power budget, this becomes a driving force for design teams to combat the spacecraft thermal loading using passive solutions rather than relying on active solutions. Though an effort is made to design the thermal subsystem with passive methods, subsystem operations and other spacecraft modes can impose conditions on the thermal design which cannot be solved passively. In such cases, active solutions need to be explored. Although active thermal solutions require power allocation, they are more effective in micro-managing the thermal loading. A thermal designer requires the knowledge of specific loading conditions that may arise during the operation of the satellite and the duration for which such conditions will prevail. To understand the loading on the spacecraft, it is important to study the interaction of the spacecraft with its environment.

The space thermal environment study will analyze the heat sources that will be affecting the satellite and the response by the satellite to this loading in the form of thermal gradients. A 6U satellite in an HEO orbit around Earth is studied. The orbital parameters like the altitude of the satellite, the inclination of the satellite concerning all applicable heat sources, and the duration of the satellite under loading and no load are studied. The response by the satellite to its environment will then be analyzed and adequate design considerations shall be made to combat conditions detrimental to satellite operation. By studying the satellite loading possible solutions can be explored making the design process streamlined.

The Foresail-2 satellite design is used for simulation of environmental interaction and Thermal solutions for the subsequent loading. The Preliminary Design of the Foresail-2 mission shall be used. Preliminary design considerations will not constitute a test-ready design of the spacecraft but will require extensive agreement with the exact thermal requirements for the subsystems. A preliminary analysis of the spacecraft could define a Trend that can be perfected upon by fine-tuning the design parameters.

2 Spacecraft Thermal Design Principles

2.1 Heat Transfer Principles

Thermodynamics deals with the transfer of equilibrium states between two thermodynamic bodies, Heat transfer differs here, in the sense, that the rate at which heat is transferred between two thermodynamic bodies is also considered. The rate of heat transfer is of great interest and importance from an engineering viewpoint [19]. It is established that heat transfer in space is dominated by conduction and radiation, convection may be present in spacecraft but for specific designs, hence omitted in this analysis[17].

2.1.1 Conduction

Conduction is the transfer of energy between particles with a thermal gradient. In solids, conduction is due to vibrations of the particle of the solid and the energy transfer through free electrons. Conduction in gasses happens due to collision and diffusion. The rate of heat transfer is proportional to the temperature difference and the area of the conducting material and inversely proportional to the thickness of the conducting material which can be mathematically represented as

$$Q \propto A\frac{dT}{dx}, \tag{1}$$

$$Q = kA\frac{dT}{dx} \qquad \text{(W)}, \tag{2}$$

where Q is the rate of heat conducted, A is the area of the conducting surface, dT is the temperature difference between the top and the bottom surface of the conducting lattice, dx is the thickness of the conducting path, and k is the conductivity of the material through which heat is transferred.

Equation 2 is called **Fourier's law** where dt/dx is the temperature gradient. Conduction is directional and directed towards lower temperature. the direction of conduction is always normal to A the area of the conducting surface[19].

2.1.2 Radiation

Electromagnetic radiation which results in heat transfer is called thermal radiation and is transported due to the energy transition of electrons, atoms, and molecules of a substance. Thermal radiation increases as the temperature of a substance increases. Thermal radiation is emitted by every material above absolute zero. The absorptivity of a material is represented by

$$E_{abs} = \alpha E_{Emitsource}, \tag{3}$$

where $E_{Emitsource}$ is the radiation emitted by the source of the radiation.

The emissivity of a grey body is given by the formula

$$E_{Emit} = \epsilon \sigma A T^4, \tag{4}$$

where, σ is the Stefan-Boltzmann constant, α and ϵ are absorptivity and emissivity respectively, E_{abs} is the energy absorbed by the body, E_{Emit} is the energy emitted by the body in the form of radiation and T is the temperature of the body[19].

2.1.3 Steady State Heat Transfer

The basis of any engineering solution can be divided into two main steps, to identify the variables involved in the physical problem along with their interdependency on each other which needs an elaborate mathematical model, which can then be solved by using an approach most suitable for providing ample exactness for the solution and also provides space for backtracing and troubleshooting. Heat transfer problems can be classified as **steady state** or **transient**. Steady-state solutions do not change with time while transient solutions do. Many of the heat transfer problems are transient in nature but can be reduced to a steady state with assumptions of certain conditions.[19].

Heat transfer can be classified as being one dimensional, two dimensional, or three dimensional. Most of the heat transfer problems in nature are three-dimensional, i.e. the heat transfer vector can be mapped along three primary axes. examples of two-dimensional problems are contours with longer dimensions along one primary axis as compared to the rest. Single dimensional heat transfer problems are those with a planar surface like glass panes where one dimension is smaller as compared to the other two[19]. In this thesis, we assume the heat transfer one dimensional for our analysis. as most of the surfaces of the spacecraft justify this assumption[19].

Assuming that the heat transfer is the only energy interaction and no energy is generated by the wall in the form of heat, the heat balance of the wall gives

$$Q_{in} - Q_{out} = dE_{wall}/dt, \tag{5}$$

where Q_{in} is the energy into the system, Q_{out} is the energy exiting the system, dE_{wall}/dt is the change in the internal energy of the wall with respect to time.

For the steady-state operation, the rate of heat flowing into the wall is equal to the rate of heat flowing away from the wall. Hence, the rate of change of the internal energy of the wall is zero. From Equation 2, we know that the rate of heat transfer is constant and the area of the wall is constant, hence we know that dT/dx is constant. the temperature through the wall varies linearly with thickness i.e. the temperature distribution in the wall under steady-state conditions is a straight line.

From Equation 2. integrating from $x = 0$ to $x = L$ we get the following eqation.

$$\int_{x=0}^{L} Q_{cond,wall} dx = -\int_{x=0}^{L} kAdT, \tag{6}$$

$$Q_{cond,wall} = kA(T_0 - T_L)/L, \tag{7}$$

where L is the thickness of the wall, $Q_{cond,wall}$ is the heat conducted through the wall, T_O is the temperature at the outer surface of the wall and T_L is the temperature of the wall at distance L. The rate of heat transfer through the wall is inversely proportional to the wall thickness and directly proportional to the conductivity of the wall material, the area of the wall and the temperature gradient between the wall surfaces.[19]

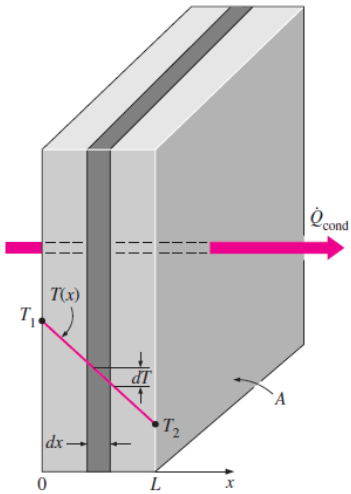

Figure 4: Temperature distribution through the wall under steady state is a straight line.[19]

Equation 7 can be reduced as

$$Q_{cond,wall} = (T_0 - T_L)/R_{wall} \qquad \text{(W)}, \tag{8}$$

where

$$R_{wall} = L/kA \qquad (^\circ\text{C/W}), \tag{9}$$

where R_{wall} is the conduction resistance of the wall. The thermal resistance of the medium depends on the geometry and the thermal property of the medium. Equation 8 is analogous to the electric current flow equation, where the heat flow can be compared to current flow, temperature difference to voltage difference and conduction resistance to current flow resistance. Similarly the radiation resistance is

$$Q_{rad} = (T_{high} - T_{low})/R_{rad} \qquad \text{(W)}, \tag{10}$$

$$R_{rad} = 1/h_{rad}A_s \qquad \text{(K/W)}, \tag{11}$$

$$h_{rad} = \epsilon\sigma(T_{high}^3 + T_{low}^3), \tag{12}$$

where Q_{rad} is the heat transfer via radiation, T_{high} is the higher temperature surface, T_{low} is the lower temperature surface , R_{rad} is the resistance to heat flow via radiation, h_{rad} is the radiation heat transfer co-efficient.[19]

Similar to circuit diagrams, thermal circuit diagrams can be drawn from the model to solve heat transfer problems of a complex multi-layered structure[19]. The spacecraft structure and components are assumed to fall under Lumped analysis. As the dimensions of the spacecraft will allow for uniform temperature distribution throughout the spacecraft, severe variation in the thermal gradient through a component is improbable. Though, certain equipment or composite surface may exhibit a sizeable amount of thermal gradient [17].

2.2 Thermal Environment Of Geocentric Orbit

The space environment as compared to surface conditions can be considered a vacuum. The ambient pressure at 100 km altitude is approximately six times lower in magnitude than that of the Earth's surface, hence a conventional heat transfer mechanism cannot be used to solve general space heat transfer problems. Owing to vacuum, the main source of heating and loss of heat in the spacecraft is radiation. Heat is transferred inside the spacecraft through conduction and radiation[16].

The heat transfer interface between the surface of the spacecraft and that of the space environment is radiation, hence the mode of heat loss from the spacecraft is via radiation[17]. The space temperature is set at a temperature of 2.7 K, calculated from the background radiation from the Big Bang [18].

The sources of heat in space in orbit around Earth can be classified as follows.

2.2.1 Direct Solar Radiation

Measurements of the solar irradiance at 1AU were carried out by NASA using the now-defunct ACRIMSAT (Active Cavity Radiometer Irradiance Monitor Satellite). The mission studied Total Solar Irradiance to provide better insight into the solar irradiance pattern. The solar irradiance depends on the distance from the sun and hence can vary seasonally. It is observed that at the summer solstice, Earth is furthest from the sun and the solar irradiance intensity is at its lowest at $1322W/m^2$ and the highest at winter solstice at $1414W/m^2$. The above values are recommended by World Radiation Centre in Davos, Switzerland, and are believed accurate within 0.4%. The solar energy is distributed as 7% ultraviolet, 46% visible spectrum and 47% short-wavelength near IR [17].

The solar radiation intensity also varies cyclically in a period of 11 years. The solar irradiance will be absorbed by the satellite surface which is under illumination which will increase the temperature of the absorbing surface. The relationship which can be used to predict the absorbed power by the surface of the satellite facing the sun is [17]

$$Q_{solar} = G_{solar}.A_{plate}.\alpha.cos\theta \qquad \text{(W)}, \tag{13}$$

where Q_{solar} is the power absorbed by the surface, G_{solar} is the solar radiation incident on the plate at the specified distance from the sun, A_{plate} is the area of the surface absorbing solar radiation and θ is the angle between the solar vector and the normal to the absorbing surface. The formula to calculate the Direct solar radiation incident on a flat plate/ solar panel is given in Equation 13. The formula depends on the area of the incident surface, surface absorptivity at the temperature and wavelength, and its inclination to the solar vector. As radiation is a surface phenomenon the intensity of the radiation is proportional to its inclination [26].

2.2.2 Earth Albedo Radiation

The solar radiation reflected back from the surface of the earth is called the albedo of the Earth. The Earth's albedo can be considered as a fraction of the solar radiation and is influenced by factors such as local solar elevation angle, cloud cover, and surface cover. The height of the satellite orbit also decides the incident albedo radiation falling on the satellite. The albedo radiation acts on the back of the satellite facing the sun and is only calculated on the dayside of the planet. Albedo from the earth can be calculated from

$$Q_{albedo} = G_{solar}.A_{plate}.a.F_v.\alpha \qquad \text{(W)}, \tag{14}$$

$$F_v = \frac{1}{A_E}\int_{A_E}\int_{A_S}\frac{\cos\theta_E\cos\theta_S}{\pi R^2}\,dS\,dE \tag{15}$$

Where a is the Earth's albedo. α is the absoptivity of the surface of the plate exposed to load, Q_{albedo} is the power absorbed by the plate due to albedo radiation, F_v is the view factor between the spacecraft and Earth. The view factor determines the fraction of radiation from the surface of the Earth falling on the surface of the spacecraft facing Earth. A_E is the radiating area of Earth and A_S is the surface of the spacecraft under loading, θ_E and θ_S are the angles between the line joining the centers of the radiating and receiving surfaces and the face normals of the radiating and receiving surface, respectively. R is the distance between the two interacting surfaces. The solar radiation falling on the surface of the earth itself is a function of the angle between the solar vector and the tangent on the point of impact[26]. The albedo radiation is maximum and assumed to be Lambertian near the subsolar point as the solar vector falls directly perpendicular on the Earth's surface. The poles also reflect higher sun light due to being snow clad. The albedo radiation reduces as the spacecraft progresses away from the subsolar point towards the terminator line and is accounted for by analysis software [17].

2.2.3 Earth IR Radiation

Incident solar radiation absorbed by Earth is emitted to space as IR radiation and thermally affects the spacecraft. Earth IR is tricky to deal with as it is similar to the IR emitted by the spacecraft (longer than that from the Sun) hence the surface layers that will reflect Earth IR will not be able to reject heat from the spacecraft. The temperature of the spacecraft could be higher than that of the effective temperature of Earth hence the spacecraft will reject heat to Earth. For ease of calculation, we assume that the spacecraft rejects heat to space (ignoring Earth) and then incoming IR is added from Earth [17]. The formula to calculate IR radiation from Earth is

$$q_1 = 237 \quad (\text{W/m}^2) \quad \pm 27 \quad (\text{W/m}^2), \tag{16}$$

$$Q_{IR} = F_v.A_{plate}.\epsilon_{plate}.q_1 \quad \text{(W)} \tag{17}$$

F_v is the view factor between spacecraft and Earth, q_1 is the energy flux at the surface of the Earth. We can observe from Equation17 and Equation15 that the Earth IR is a function of the altitude of the spacecraft.

2.3 Thermal Design Principles

The spacecraft thermal control design aims to maintain the temperature (including fluctuations and worst-case conditions) throughout the spacecraft under a predefined range. The range that the thermal control has to perform under is decided by comparing the temperature window in which the spacecraft components will be able to work in their optimum condition. The idea of the subsystem components will help in designing the optimal operating range of the spacecraft.

2.3.1 Spacecraft Heat Balance Equation

A preliminary study of the spacecraft can be performed to understand the general temperature profile of the spacecraft by performing a steady-state analysis. Steady-state will be reached when The incoming load on the spacecraft is equal to the heat lost by the spacecraft. This will give us a general trend of loading on the spacecraft under equilibrium. according to Kirchhoff's Law

$$Q_{in} + Q_{internal} = Q_{out}, \tag{18}$$

where Q_{in} is the incoming heat load on the spacecraft, $Q_{internal}$ is the internal loading on the spacecraft and Q_{out} is the heat lost by the spacecraft to the surrounding.

The sources of spacecraft heating are direct solar radiation, Reflected albedo loading from Earth, and IR radiation from the Earth. Very high altitude orbits will also face Albedo and IR radiation from the moon. In an HEO orbit, the distance between the satellite and the Moon will not be substantial enough such that the moon albedo and IR will affect the spacecraft, hence the Moon is not included in the analysis. From Equations 13 14 17, we can write change equation 18 as

$$Q_{in} = Q_{solar} + Q_{albedo} + Q_{IR}. \tag{19}$$

In Equation 19, Incoming heat from Earth IR will practically be negative with surface properties of the spacecraft used for the equation solution, as spacecraft temperatures are generally higher than Earth in most cases.
The heat lost from the spacecraft can be calculated from the Equation 4, where the surface facing the space environment will be the one to lose heat

2.4 Heritage Missions

Heritage missions are an important asset in designing a spacecraft. Heritage missions are missions with similar mission design requirements and have successfully been able to perform a technological demonstration for the systems being used. Hence heritage missions act as a test in itself for various technologies and hence these technologies can be incorporated with a high level of trust.

- GTOsat is a 6U CubeSat by NASA Goddard space flight center, USA, to GTO. The spacecraft will act as a pathfinder for the more radiation-resistant robust version of the Delingr-X hardware in an attempt to establish foundations of smaller satellite launches to higher altitudes. The scientific payload includes a spectrometer (Van Allen Probe) to study the interaction with solar winds and the loss of the electron from the energetic particle belt.

- SpectroCube is a 6U CubeSat planned to be launched to HEO. SpectroCube carries a spectrometer to measure photochemical changes of organic molecules, which will be important as bio-markers for the detection of life in the solar system and beyond.

- The foresail-1 mission is a 3U CubeSat mission to LEO by Aalto University and the Finnish Centre of Excellence. The Payloads include PATE and the Plasma Brake Experiment. The foresail-1 mission is the spiritual successor for the Foresail-2 mission, which is a 6U CubeSat planned to be launched into an HEO/GTO orbit.

None of these missions have been launched yet and unfortunately, no publishes of the design of the subsystems for GTOSat and SpectroCube have been found. Hence, though the importance in keeping up to date with these missions is noted, these missions will not help this thesis extensively at the time of its writing.

The foresail-1 mission will be used as a heritage mission to replicate mission design parameters that stay constant through both missions. The Foresail-1 and Foresail-2 missions will be designed and manufactured at Aalto university Finland, and hence will enable ease of technology transfer and reproduce-ability between the two missions. The Foresail-1 and Foresail-2 missions also share the plasma break experiment which will put constraints on both missions in a similar fashion. The thermal design of the Foresail-1 mission may not replicate for the Foresail-2 mission as the orbital parameters, scale and payloads vary to various degrees between the missions.

3 Geocentric Orbit Thermal Environment

The Spacecraft's orbit determines the thermal loading on the satellite. The loading on the satellite will be cyclic and the loading cycle is defined by the orbital route of the satellite. The orbit determines conditions like sun exposure timing, albedo, and IR load timings, and eclipse conditions. To get a basic idea of the impact of the orbital parameters on the satellite we perform black body radiation analysis of the satellite. The satellite is considered as a black body and its response is analyzed for the orbit. This shall give us the maximum and minimum loading conditions, their occurrence, and seasonal loading profile. This can be used to model the spacecraft loading and the loading on the mathematical model of the spacecraft to find the most suitable thermal solutions to meet requirements.

3.1 Black Body Analysis

Radiation is the primary heat transfer mode in space which occurs through the external surfaces of the spacecraft exposed to space conditions. Owing to the cost-effectiveness of surface coatings and its ease of operation, it is the norm for engineers to check for passive solutions for spacecraft loading. Various surface finishes produce different loading profiles on the spacecraft. It is time-consuming to model all of these surfaces individually to find the most ideal surface finish. A general understanding of the orbital conditions can indicate cases of loading which can be averaged for the entire orbit and solved. This will greatly improve the time consumed in the design process. Hence to understand the general conditions that can be expected in orbit and a general idea of which direction the design engineer should look towards for the thermal solution, a pilot solution needs to be chalked. Black Body analysis of the spacecraft model aims to provide the engineering team with specific loading conditions that will pose a challenge for the spacecraft during orbit. It is possible that such loading anomalies can be overlooked during the analysis of the spacecraft with its design parameters. Black Body analysis appropriately identifies loading on the spacecraft due to external sources and does not involve manipulation in loading due to design parameters like surface finish and internal loading.

Black body absorbs all the incoming radiation. Black Body analysis deals with the response to thermal loading of a black body model. The aim of the black body analysis is to find the loading on a model without the interference of model components such as the thermal properties of the material and the thermal inertia of the solid model. Such parameters could hide loading trends in orbit which may be of critical importance in other missions or experiments. Hence, to find the exact loading trend in orbit, we use a black body model and observe its loading. We aim to achieve the heating and cooling trends in the model throughout the orbit to find conditions that stand out or are unique.

The Black body analysis is performed on a CubeSat with dimensions 120x360x240

mm (standard 6U CubeSat). The CubeSat is in a prograde orbit around Earth with its velocity vector parallel to the positive Y-axis and the negative X-axis pointing towards Nadir. The X-Z side is the largest and the X-Y side is the smallest in surface area of the sides of the satellite [24]. NX space systems Thermal solver is used to perform the analysis to find the orbital heating in the selected orbit. The model is a 2D mesh of the surface of The spacecraft as radiation is a surface phenomenon. The analysis will give simulations for the heating on the surface of the spacecraft and not inside the spacecraft, i.e. The loading on the spacecraft due to radiation and not conduction through the surface inside the spacecraft. The thermo-optical properties were assumed to be that of a perfectly black body. The Apogee and Perigee altitudes are 36000 km and 400 km respectively. The RAAN and the Inclination of the spacecraft are assumed to be 0°. The Orbital period of the satellite is 38331 seconds per orbit for the assumed orbital conditions. Figure 5, Figure 7, Figure 9 and Figure 11 represent the temperature graph of the spacecraft in respective orbital seasons.

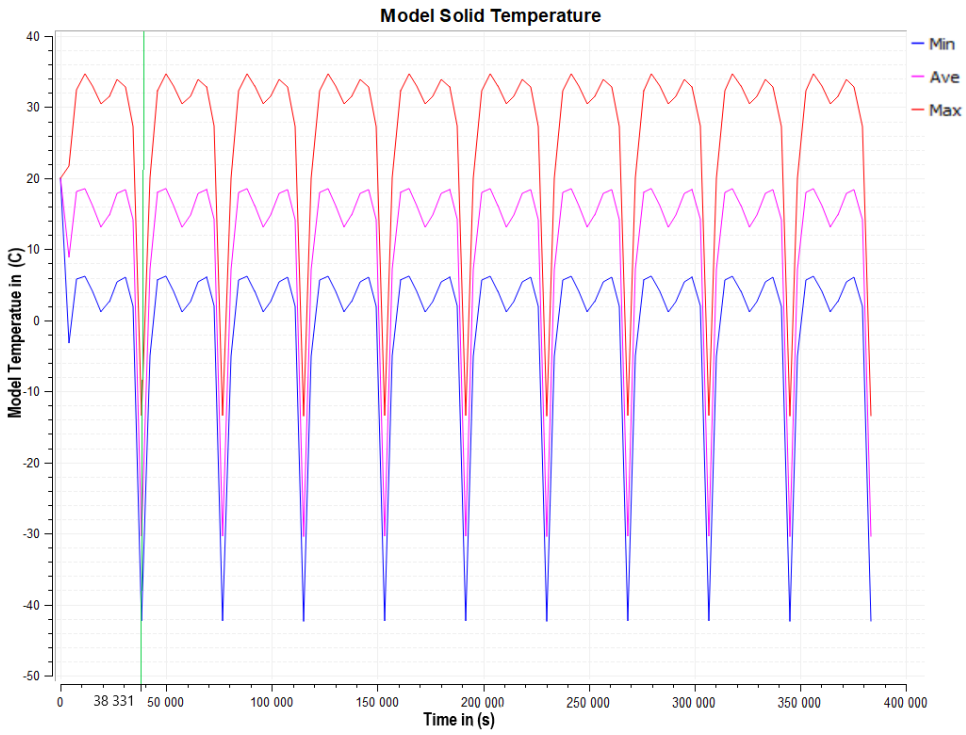

Figure 5: Black Body temperature profile of a 6U spacecraft structure in June Solstice orbital seasons

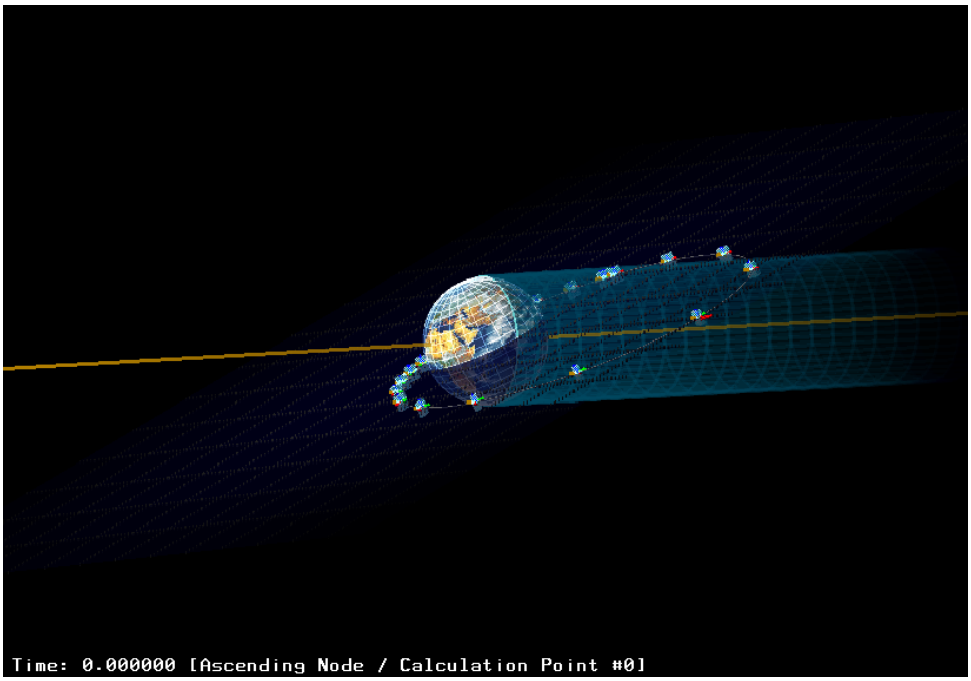

Figure 6: Orbital path of a 6U spacecraft structure in June Solstice orbital seasons

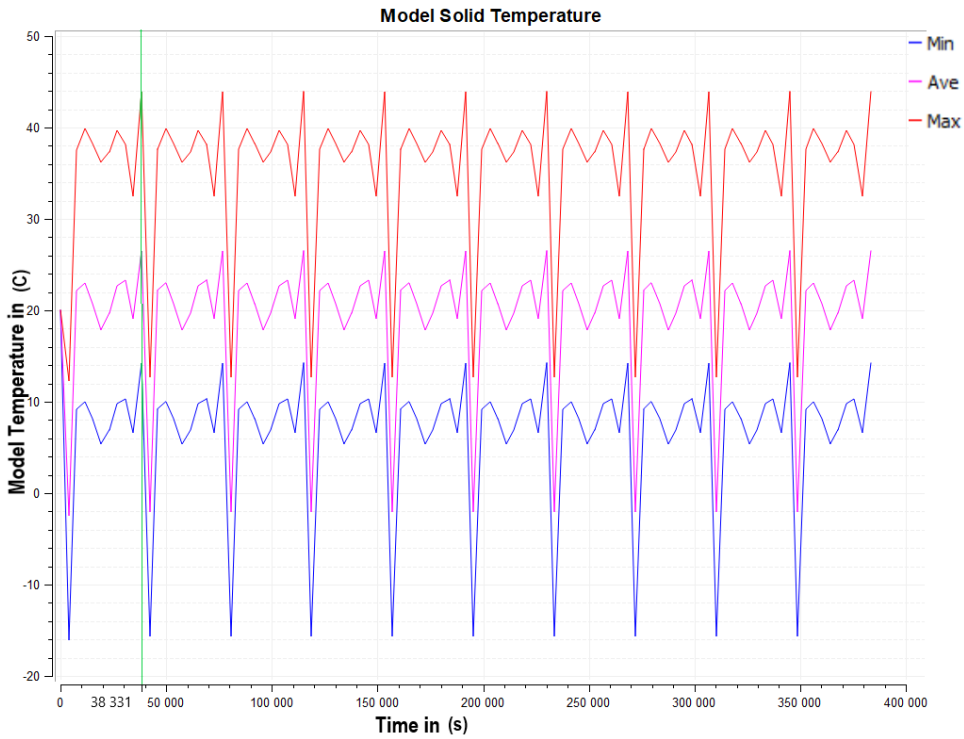

Figure 7: Black Body temperature profile of a 6U spacecraft structure in December Solstice orbital seasons

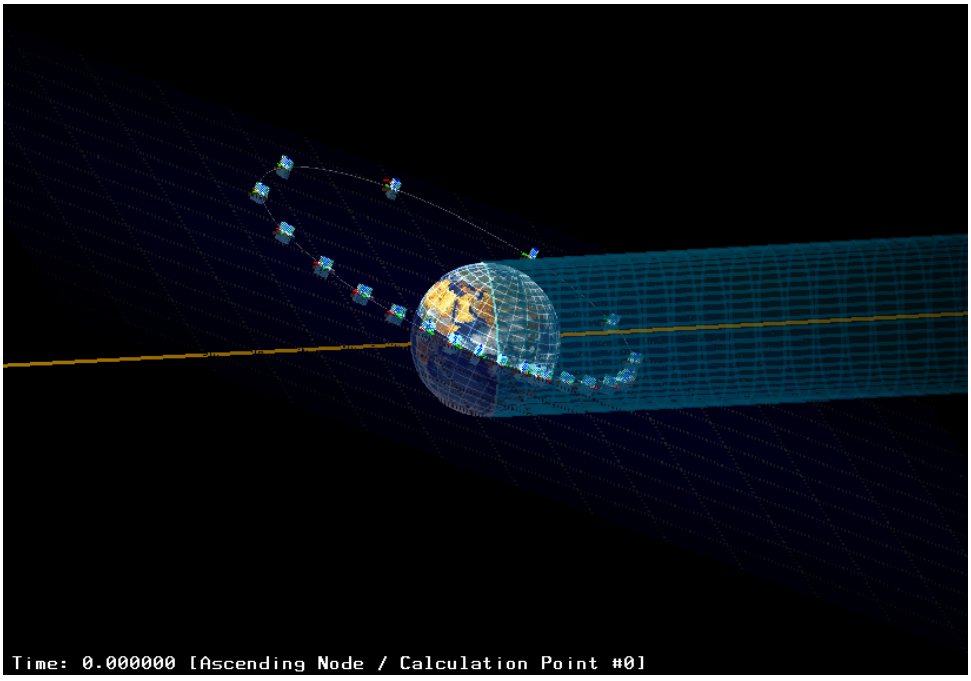

Figure 8: Orbital path of a 6U spacecraft structure in December Solstice orbital seasons

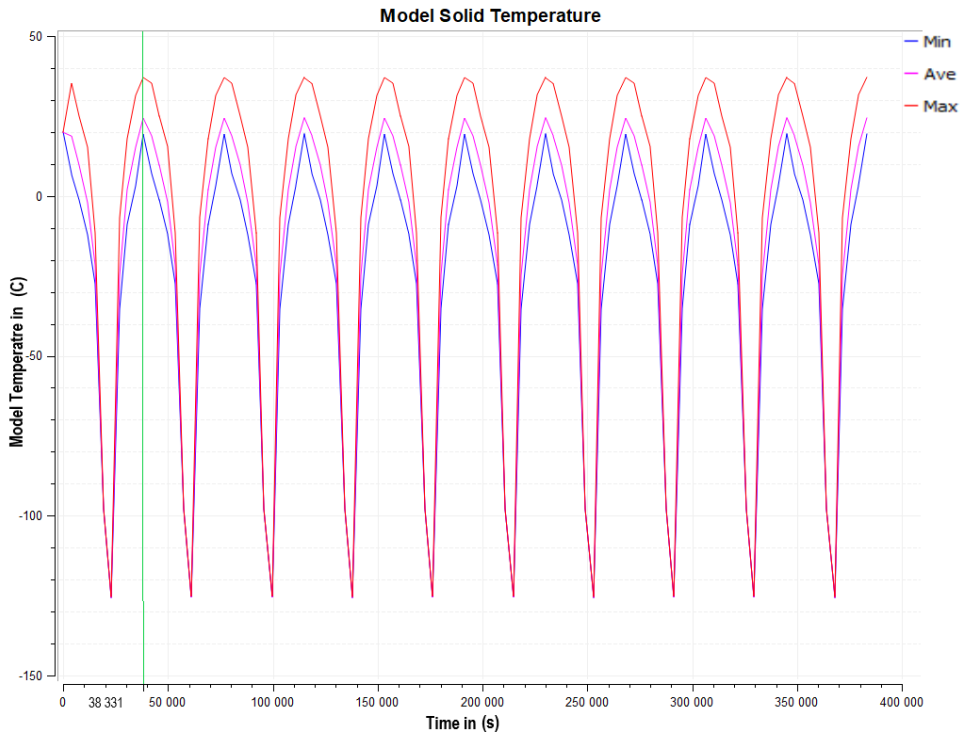

Figure 9: Black Body temperature profile of a 6U spacecraft structure in March Equinox orbital seasons

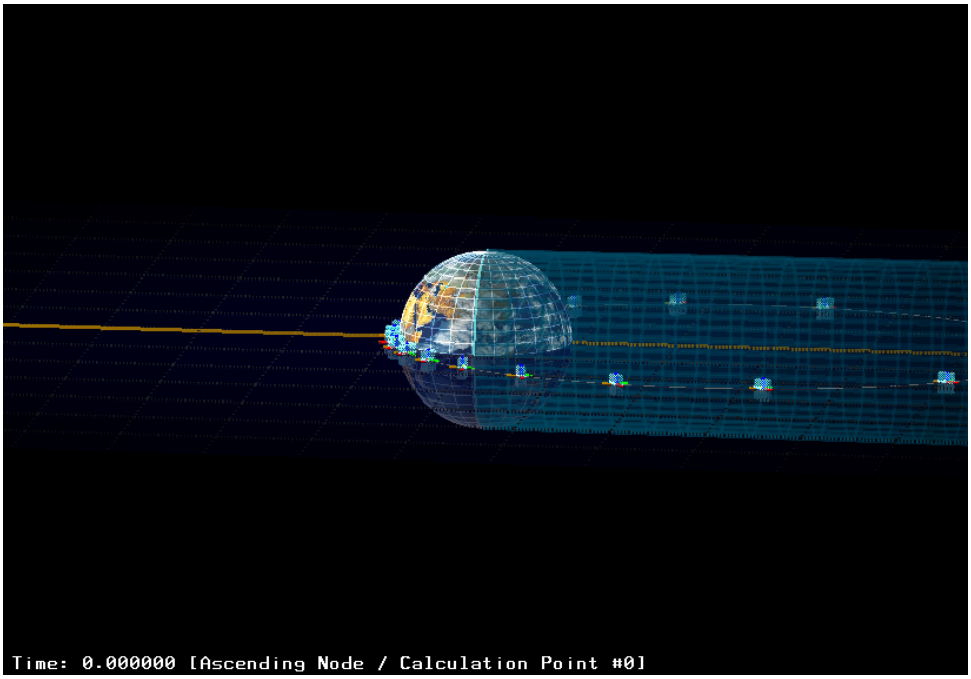

Figure 10: Orbital path of a 6U spacecraft structure in March Equinox orbital seasons

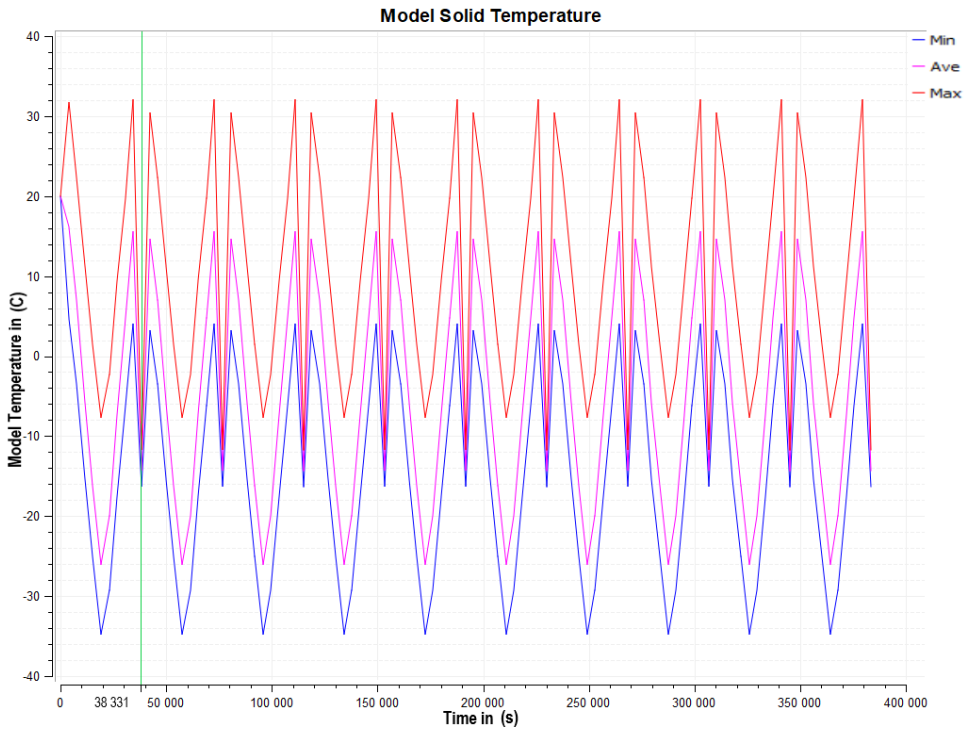

Figure 11: Black Body temperature profile of a 6U spacecraft structure in September Equinox orbital seasons

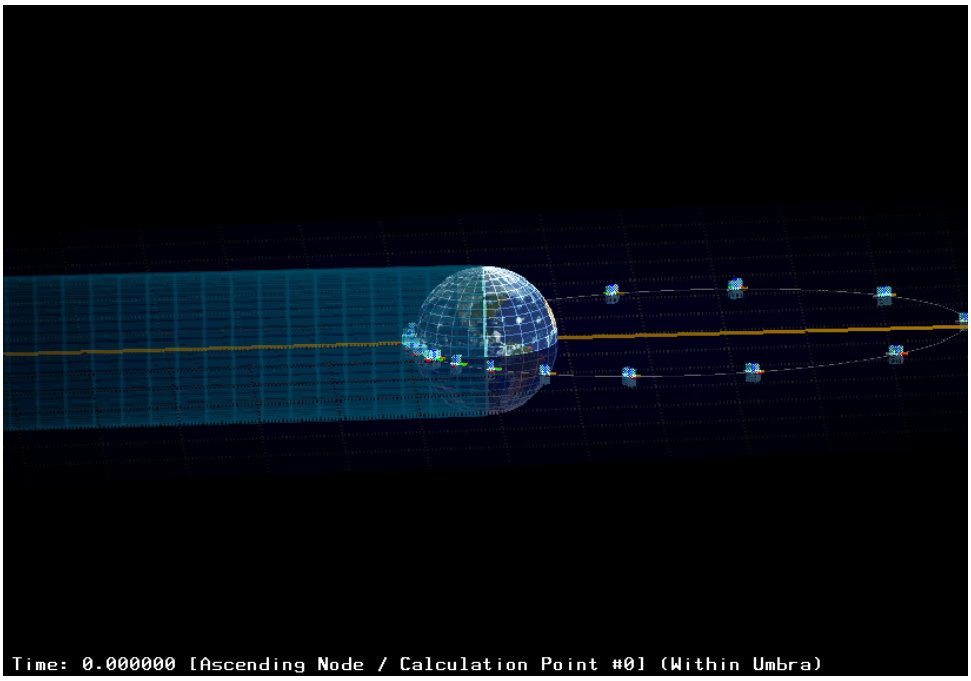

Figure 12: Orbital path of a 6U spacecraft structure in September Equinox orbital seasons

Transient analysis was performed for ten orbital cycles. Twenty transient iterations per orbit were selected and solved for. The temperature graphs for the maximum average and minimum temperatures were plotted.

The black body analysis shows the maximum and minimum loading on the spacecraft. The maximum warm loading is observed during December Solstice and the maximum cold loading is observed during March Equinox. The thermal cycling on the spacecraft can also be seen for various seasonal conditions. The severe drop in the temperature for March Equinox is because the apogee of the spacecraft orbit falls inside the umbra of the Earth. Hence the spacecraft has to navigate through a region of almost zero thermal loadings (except for internal loading) for an extensive period of the spacecraft orbit. Similarly, for December Solstice it can be observed that the temperature graph is jagged. This is partly because the solar radiation falling on the spacecraft takes effect as soon as the spacecraft moves into solar illumination from the eclipse. The peak temperature for a particular season is approached at the end of one orbit as the maximum loading on the spacecraft is when the spacecraft position is near Earth. The peculiar loading pattern during the solstices is because of the geometry of the spacecraft and the satellite pointing during the orbit. As the satellite will be facing the sun with its largest side while approaching and departing from the perigee and apogee conditions, and it is comparatively narrower face while reaching perigee, there is a noticeable dip in the temperature of the spacecraft. It can also be observed that there is a very low loading on the spacecraft in March Equinox(longest spacecraft eclipse orbit).

We can observe that the spacecraft will undergo extreme temperature drops in the orbit owing to the large duration of eclipse conditions in orbit. The eclipse duration will be the longest during the March equinox. Also, factors affecting the satellite is that in higher altitudes the spacecraft will only be affected by the Sun acting as a heat load hence diminishing the heating on the satellite that will otherwise be from the Albedo and the Earth's IR. The profile of the spacecraft loading can also be observed from the temperatures graphs representing the response in different orbits. The loading graph is exclusive for orbital conditions, while it can be generally observed for orbits similar to those assumed for the analysis, the graph will tend to deviate from those observed as the orbit become more dissimilar, even though the altitudes may remain the same, and will also be affected by the satellite orientation.

3.2 Spacecraft Loading

Thermal Loading on a Spacecraft refers to the temperature gain by the applicable satellite surfaces due to various sources of heat encountered in the satellite orbit. The impact of the changes in altitude and orientation of the satellite orbit plays a major role in the loading of the spacecraft. As the satellite is in an initial design phase, the study of this impact can provide some insight to the spacecraft design engineer. The analysis setup uses a unit surface with area m^2.

3.2.1 Incident Solar Loading

The formula to calculate the Direct solar radiation incident on a flat plate/ solar panel is given in Equation 13. The orbital parameters are unchanged and for ease of calculation, RAAN is assumed to be 0°. Given the orbital inclination range, the inclination of the plate concerning the sun vector varies from -23 degrees to 7 degrees. From the Equation 13, the area of the plate is taken as unit area and the absorptivity as a unity which will give us the solar power flux as a function of inclination. The inclination was selected so that the maximum loading condition can be simulated.

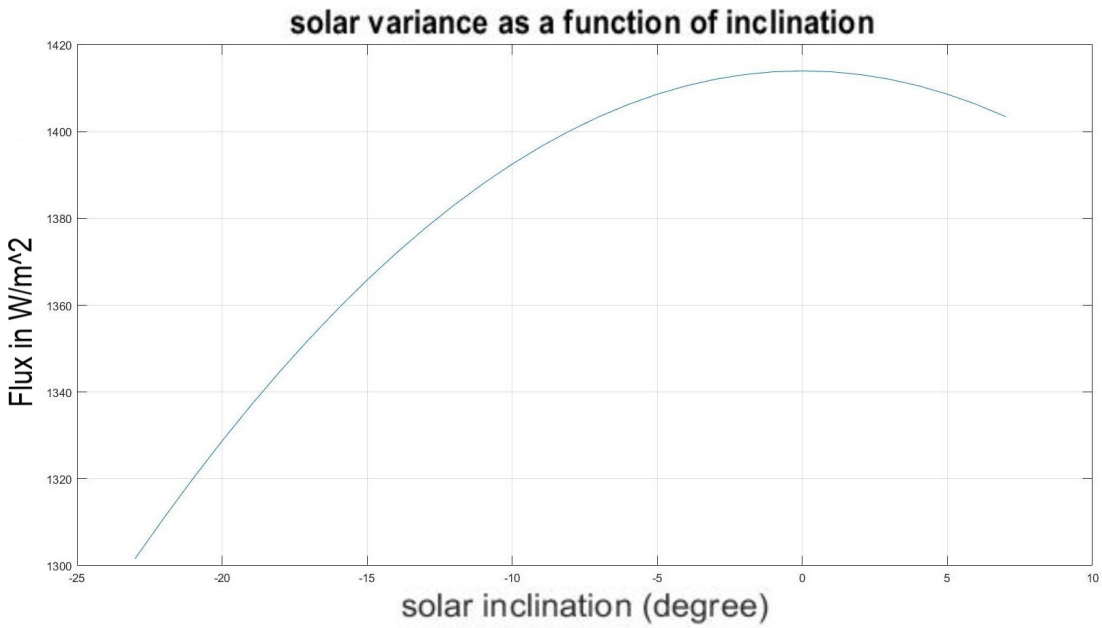

Figure 13: Solar Flux as a function of Inclination of the spacecraft dependent on the face normal to the spacecraft surface and the solar vector

The simulation results show the change in the loading of the spacecraft based on the inclination of the satellite orbit. We assume that the satellite orientation concerning the velocity vector and the nadir vector is the same for all inclinations. we can observe that the solar radiance is maximum when the inclination of the spacecraft is the same as the solar declination angle i.e. 23.45°. As the satellite face is normal to the sun vector, maximum loading occurs on the satellite, while as the angle between the satellite surface normal and the sun vector increases the loading on the satellite decreases. We assume that the plate is normal to the sun vector when the orbital angle is the same as the solar declination, else the loading will depend on the cosine of the angle between the solar vector and spacecraft surface normal facing the sun. The slope of the graph indicates the reduction in the loading on the spacecraft based on the inclination angle concerning the sun vector. The spacecraft model is assumed to have black body thermo-optical properties. The loading is calculated on MATLAB and the satellite dimensions are not changed from before.

3.2.2 Earth Albedo Loading

From Equation 14, we can see that the albedo loading depends on two factors. The percentage of solar radiation reflected from earth, represented by a, and the view factor of the spacecraft, F_v. The albedo a varies depending on surface cover, cloud conditions and the position of the spacecraft in orbit.The albedo radiation varies throughout the orbit of the satellite and can be difficult to pinpoint. The NASA/Marshal Space Flight Centre (MSFC) study to find the earth's radiation budget using the Earth Radiation Budget Experiment (ERBE) was a mission which used three satellites, one earth radiation budget satellite and two National Oceanic and Atmospheric Administration satellites, to observe the radiation budget of Earth. This study is cited by [17] for the tabulated albedo values. Of these, we will only be looking at 3.3-σ albedo values(see table 3). These values for albedo are exceeded only 0.04 percent of the time for the given time period.

Time Period (s)	Albedo (Cold Case)	Albedo (Hot Case)
16	0.06	0.43
128	0.06	0.42
896	0.07	0.37
1800	0.08	0.33
5400	0.11	0.28
21600	0.14	0.23
86400	0.16	0.22

Table 3: 3.3-σ albedo values for hot and cold case conditions for an orbit inclination of 0-30 degree [17]

The albedo value can be selected from the list shown in table 3. The Hot case and cold case albedo values are tabulated. When designing hardware with certain thermal time constants, the albedo value for a similar time period can be selected from the table. Albedo values are reported for inclination of the satellite between 0 to 30 degrees. These values of orbital inclination are selected from [17] because they are the most relevant for this study.

The altitude of the satellite influences the view factor of the satellite (Equation 15) and therefore also the albedo load (Equation 14) . The view factor is inversely proportional to the square of the distance between the radiating surfaces. The increase in altitude causes the albedo load on the satellite to decrease hence causing the satellite to be colder. This variation needs to be accounted for during the heat balance of the satellite.

The albedo selection and view factor calculation for this study are done by the NX software's space systems thermal solver environment. The values from the ERBE study are provided for reference only.

3.2.3 Earth IR Loading

The graph of the earth IR on a unit plate as a function of the spacecraft altitude is mapped in Figure 14 using Equation 17. The plate of unit surface area and perfect black body emissivity are assumed.

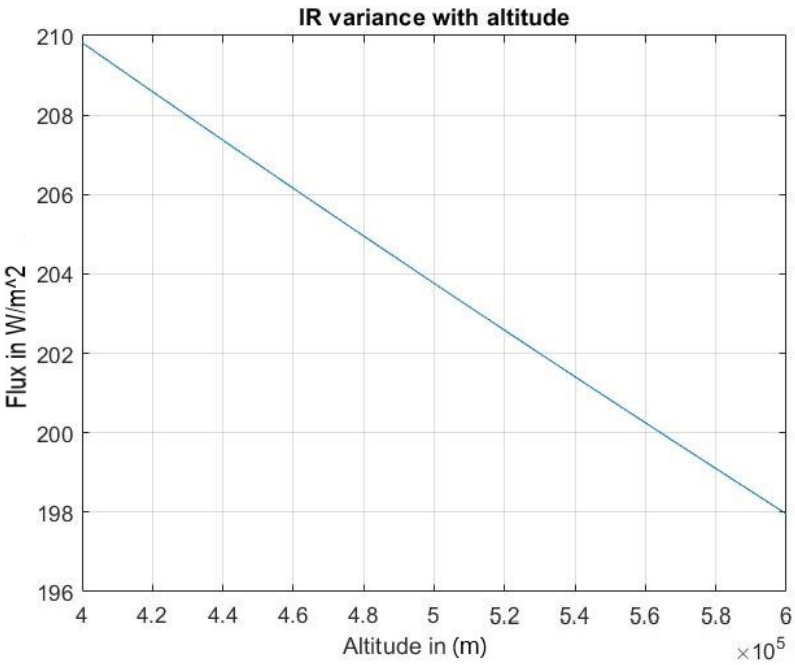

Figure 14: IR power on a unit plate as a function of spacecraft altitude

From Figure 14 it can be observed that the IR power from the Earth falls linearly as the altitude increases. From Equation17 and Equation15 the IR radiation is dependent on the view factor between the spacecraft and Earth . As Earth IR will be affecting the spacecraft throughout the flight, the variation of the IR needs to be accounted for during spacecraft thermal design. Maximum and minimum IR loading on the spacecraft needs to be identified and the thermal solution tested for both conditions.

3.2.4 Seasonal Loading

The seasonal loading on a 6U satellite in the orbit specified was performed and the simulation results were plotted. We can observe the loading on the satellite faces in orbit for four seasonal conditions. The loading on individual Finite Elements was observed and graphs for the same were plotted. Selected elements represent the average loading on that face. The nodes and their corresponding perpendicular satellite body axis is shown in Table 4.

The loading on the spacecraft includes heat from all the applicable sources viz. the sun, the reflected radiation from Earth's surface, and the Earth IR radiation to the spacecraft (If applicable). The simulation objects included the orbital heating of the spacecraft and the radiation environment of the spacecraft. The simulation results for the spacecraft show the loading intensity on the spacecraft face elements. The maximum heat loads are observed in the face's normal parallel to the X-axis and the element facing towards the positive X-axis of the spacecraft body axis. This is the spacecraft face facing zenith. As the maximum loads on the spacecraft are due to the solar radiation falling on the spacecraft surface the surface facing the sun will have the maximum loading. The plates perpendicular to the Z-axis are facing loading during solstices as the inclination of the Earth to that of the sun is prominent during this orbit for the orbital inclination of 0°. similarly, the faces perpendicular to Y-axis are facing loading depending upon which face is under solar illumination during the leading and trailing path from the vertices of the orbit.

Orbital season	CAD elements perpendicular to respective Spacecraft axis					
	X_+	X_-	Y_+	Y_-	Z_+	Z_-
June solstice	139	7	101	29	90	67
December solstice	139	7	101	24	82	66
March equinox	139	7	96	24	83	76
September equinox	150	7	96	24	83	76

Table 4: CAD model elements and their corresponding spacecraft body axis orientation

Figure 15 and Figure 16 represent the heat loads on the spacecraft during the four major orbital seasons. The elements in the figures represent surfaces of the spacecraft normal to the spacecraft axes as shown in Table 4.

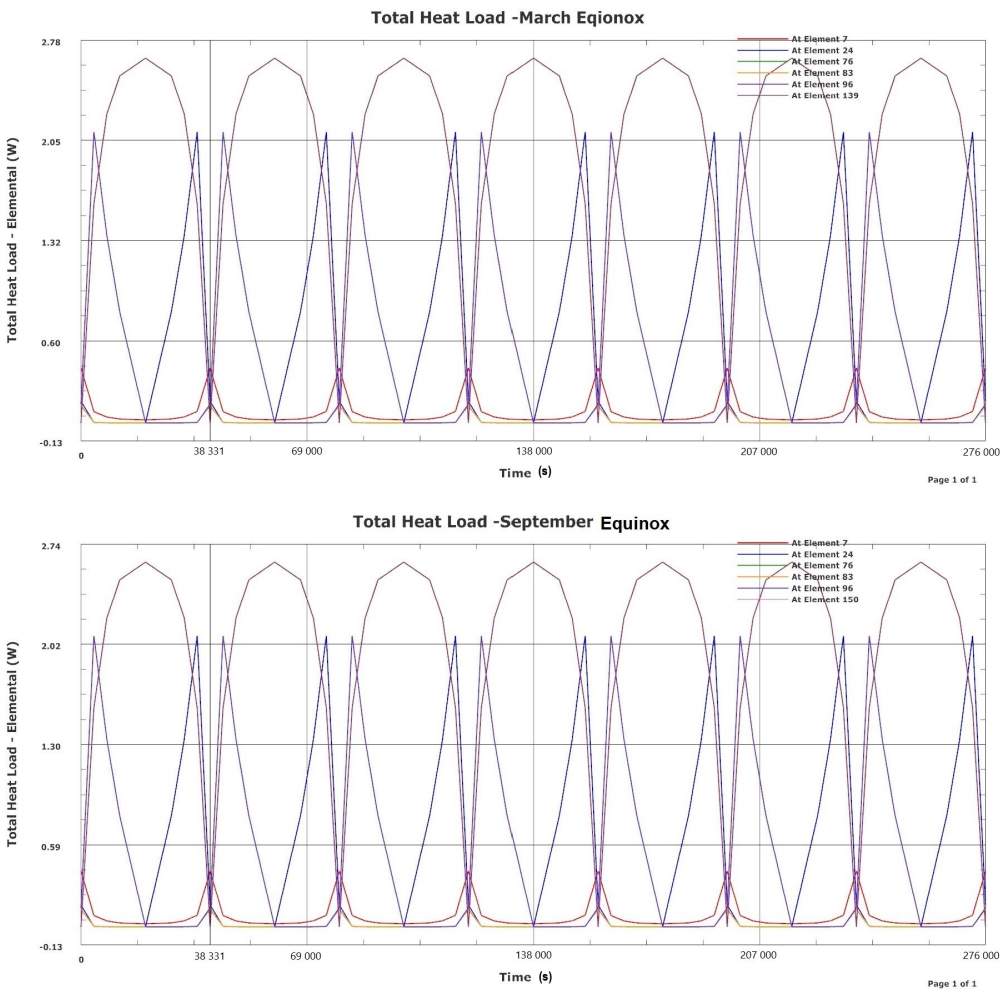

Figure 15: Heat Loads on face elements in March and September equinox orbital seasons

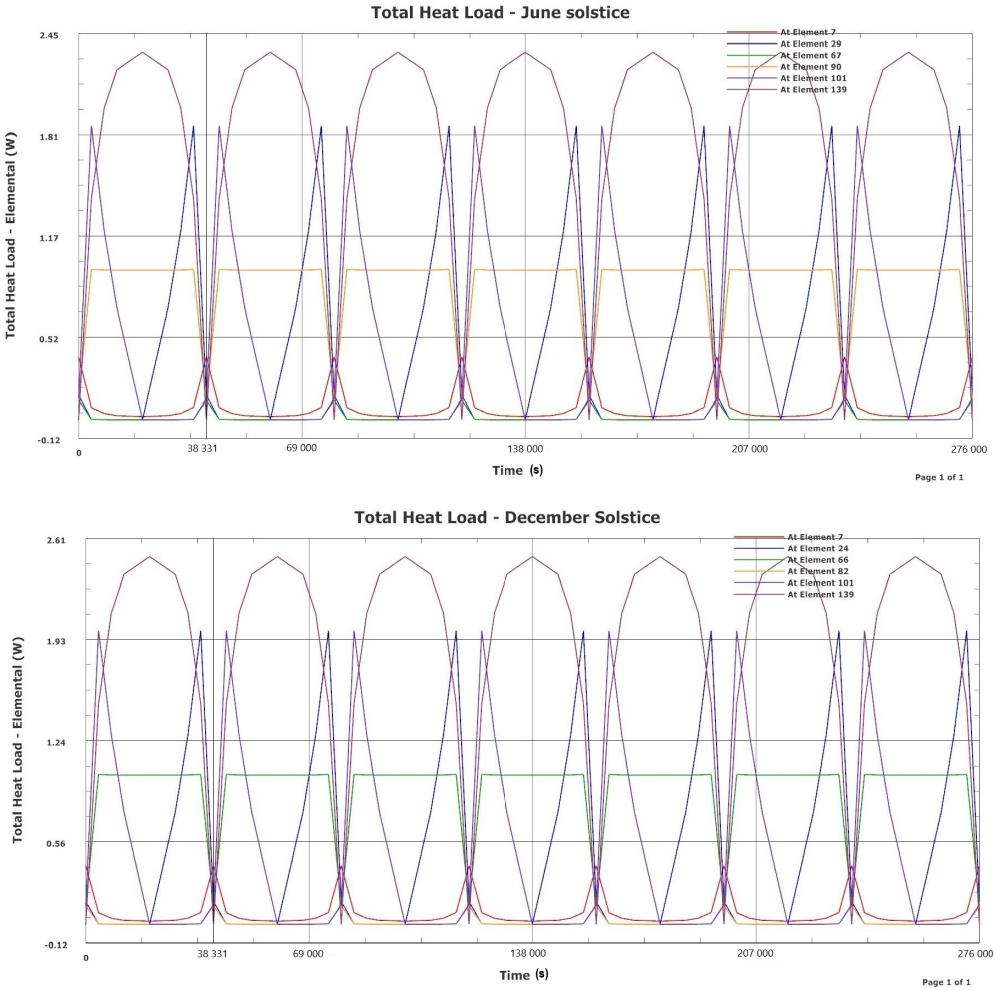

Figure 16: Heat Loads on face elements in summer ans winter solstice orbital seasons

3.3 Inclination Of The Spacecraft Orbit

The spacecraft loading depends on the illumination of the spacecraft, which is reliant on the spacecraft orbital parameters. The inclination of the spacecraft is one of these parameters which shall dictate the loading on the spacecraft. The inclination of the spacecraft will influence the time the satellite will be in loading and shadow under the Earth's umbra. The change in the inclination of the spacecraft orbit will cause changes in the incident angle of the incoming radiation hence changing the loading.

The spacecraft was modeled in NX and the orbital heating simulation was performed to study the impact of varying orbital inclination on the spacecraft in an HEO scenario. The model is a CubeSat with 6U dimensions and the body was assumed to be a perfectly black body. The satellite model meshed as a 3D solid. The orbital inclinations were varied and the average temperature of the spacecraft was plotted. The inclination angles assumed for the simulation were $0°C$, $5°C$, $10°C$, $20°C$, $30°C$. The RAAN is assumed to be 0°. The angles for the analysis are selected according to the orbital inclinations of interest for the foresail-2 mission and will be the focus of the study.

The graphs show the loading on the model for the angles $5°C$, $10°C$, $20°C$, $30°C$. It is observed that the temperature of the spacecraft model decreases until 20 deg orbital inclination, and increases afterward. As the inclination of the spacecraft increases the time spent by the spacecraft under illumination increases. This increases the loading on the spacecraft in return increasing the temperature of the spacecraft. As the spacecraft inclination reaches the value of 23.45 $°C$, the β angle reduces to zero. This means that spacecraft orbit will be in a path with the least amount of illumination. This is less prominent during equinoxes but is still observed.

Inclination in degrees	**Summer solstice in °C**		**Winter solstice in°C**	
0	4	-8	9	-5
5	4	-11	9	-7
10	0	-13	6	-10
20	-6	-20	0	-16
30	-4	-17	2	-1

Table 5: Solstice maximum and minimum temperature for varying inclination

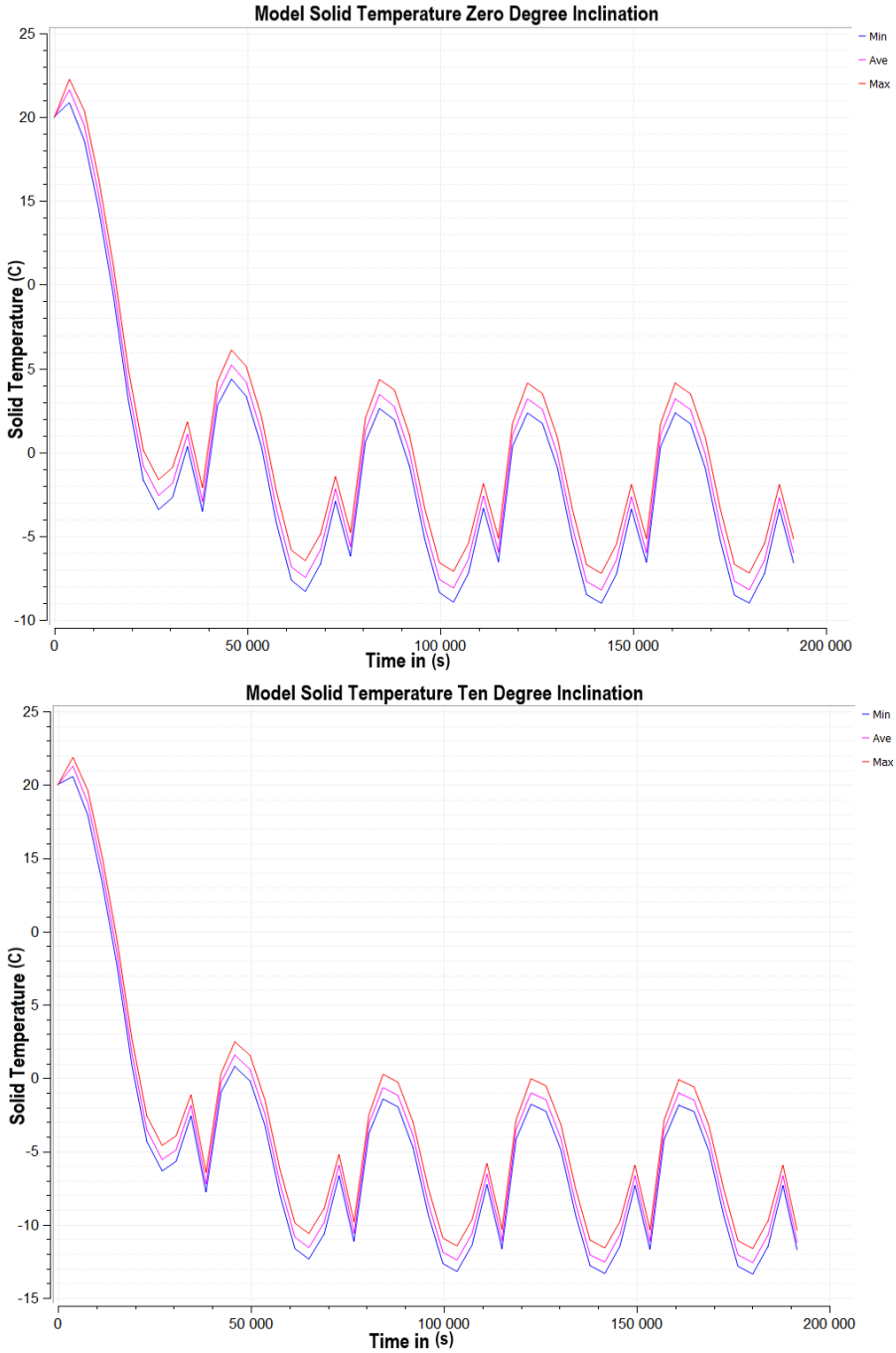

Figure 17: Temperature profile of 6U spacecraft in summer solstice Orbital season with Orbital Inclination of 0° and 10°

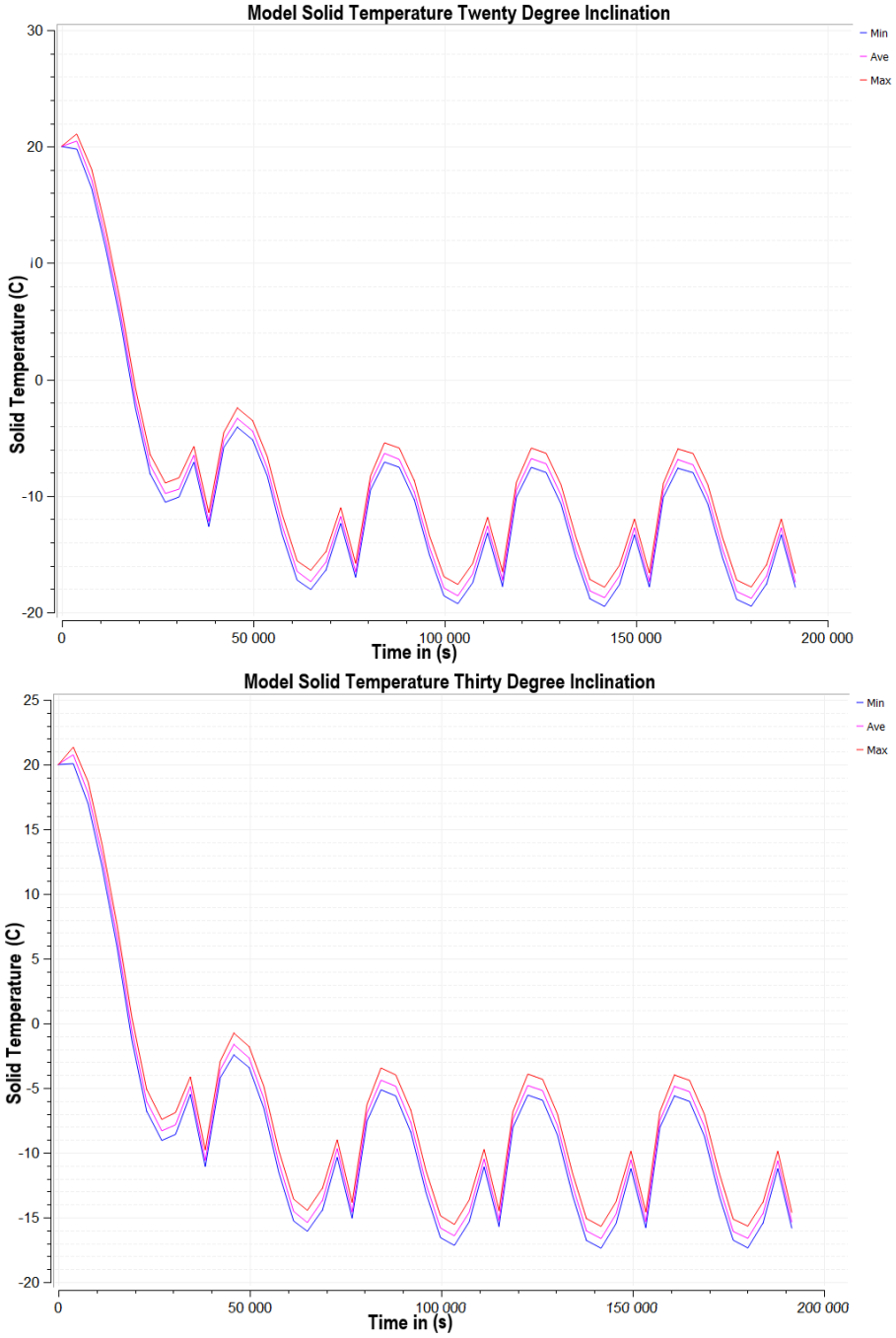

Figure 18: Temperature profile of 6U spacecraft in summer solstice Orbital season with Orbital Inclination of 20° ans 30°

3.4 Loading On A Rotating Satellite

Rotating satellites will differ in heating from non-rotating satellites. Multiple faces will be under solar radiation load for periods corresponding to the rotation of the satellite. Satellite rotation could increase the cooling load, induce thermal stress across faces and cause damage, hence it is important to know the loading profile on the surfaces of a rotating satellite. Graphs were plotted for the loading on the rotating satellite for increasing rotation rates, to study the loading profile on it. For the study, a unit plate was selected to simulate the loading on a single satellite. The area under the curve was also studied to see the total loading on the satellite.

A rotating satellite will have uniform heating of the satellite surfaces coming under illumination as compared to a non-rotating satellite, where only the surface under illumination will be heated by radiation. The rotation causes cyclic loading on the satellite and could cause mechanical damage as a result in certain materials and configurations, and needs to be addressed.

Fourteen rotation rates were selected to analyze the rate of heat transfer to the plate for varying rotation rates. The selected rate of rotations per minute were 0.15, 0.176, 0.2, 0.23, 0.3, 0.43, 0.6, 0.99, 1.5, 3, 6, 10, 15 and 30. The graphs for the loading on a unit plate were plotted for a period of one minute and compared. The plot follows the profile of a cosine wave and the negative trough of the wave will be ignored. The Negative part of the wave is ignored as the source of heating (The sun in this case) is acting on only one side of the plate. The area under the curve for the individual varying RPM plots was calculated to get the total energy gain by the plate for all individual cases. Observing the area under the curve certain observations were noted. The plot follows a pattern of occasional peaks that diminish gradually. Between the peaks, the temperature reduces before increasing gradually. In the set, the maximum peak was observed at 0.43 rotations per minute. The loading on the plate is maximum when the plate is directly under the solar radiation with a minimum angle between the plate normal and the sun radiation vector. Rotation causes a drop in loading which increases gradually as the rate of rotation increases. The graphs can be observed in Appendix A

4 Foresail-2 Design Overview

The Foresail-2 mission designed and manufactured by Aalto University, Finland, is a 6U CubeSat carrying payloads to study energetic particles in the Van Allen belt and the proof of concept for using the Coulomb drag to reduce the satellite altitude. Foresail-2 satellite will have three payloads, a Magnetometer, a Plasma Break experiment, and REPE, a particle detector. The lifetime of the satellite operations is six months and the satellite will use Plasma breaks to deorbit.

Apart from the payloads, the satellite will have platform subsystems. The spacecraft includes the Avionics stack, The propulsion/ attitude maintenance subsystem, and the power subsystem along with the TTC subsystem. Previous sections discussed the operational temperature ranges of general subsystems and the same shall be assumed for Foresail-2. The power budget of the spacecraft is unclear but the assumptions made for the Foresail-1 mission can be scaled to meet the requirements for the Foresail-2 mission. It is assumed that the Foresail-2 mission will have body-mounted solar panels covering all the sides of the satellite. The satellite will be rotating about an axis in orbit hence to maximize the harvesting of the solar energy, the satellite will have to have body-mounted solar panels. The Power subsystem needs to be robust to account for the rotation of the satellite and the possibly longer eclipse conditions Than Foresail-1.

Suggested values of 3931.2 rotations per orbit were selected for the satellite [24]. The rotation of the satellite causes higher thermal cycling on the surfaces of the satellite and impacts the loading on the satellite. This complicates the thermal design process and also poses restrictions on passive cooling solutions. The comprehensive thermal design of the spacecraft at the current stage of development is premature and might not be relevant as the design progresses, yet a general trend towards satellite thermal design is touched upon. Assumptions where necessary are made and the thermal consideration for the spacecraft design and studies are performed.

The solar panel assembly is similar to the Foresail-1 mission. Gallium arsenide solar cells are mounted on FR4 substrate using silicone adhesives/Kapton tape. The substrate is covered with a surface covering with properties most conducive for the loading on the satellite. The solar panel is covered with tempered glass to reduce surface degradation due to orbital conditions. The surface of the spacecraft structure is anodized, the optical property of the anodized surface is similar to that of the Foresail-1 mission. The satellite rotation is around Y axis and the velocity vector direction is parallel to the positive Y axis. The orbital properties are retained from the Black body thermal loading analysis.

5 Spacecraft Thermal Design Consideration

The observations made in the environmental interaction study will be applied to the Foresail-2 mission. The preliminary thermal design of the spacecraft in the specified orbit is studied and the various design critical aspects are discussed. Assumptions for the study are made per the Foresail-2 design, but the final design may or may not follow the pattern studied here. The Foresail-2 mission design is in the preliminary design phase as of when the study of this thesis was conducted, hence the inferences obtained here are representative of a starting line for the thermal study rather than a robust thermal design ready for testing.

5.1 Surface Coatings For GTO

The spacecraft surface is the primary surface for heat transfer. The surface of the spacecraft comes in contact with the incoming heat loads and the space thermal environment. The thermo-optic properties of the external surface of the spacecraft will affect the loading on the spacecraft. Influencing the surface properties of the spacecraft can result in desirable loading profiles. Various surface finishes exist which can be used for specific loading conditions.

The Foresail-2 mission model is a 6U CubeSat with body-mounted solar panels covering all sides. The solar panel design follows the Heritage Foresail-1 mission. The solar panel is mounted on an FR4 substrate which is mounted onto the structure of the spacecraft using screws. The structure of the satellite is a honeycomb structure made from Aluminium which will be anodized using the same method as that of the Foresail-1 mission structure. The FR4 material will be covered by an appropriate surface finish so that desired temperature ranges may be observed. The structure of the spacecraft is Aluminium black anodized. The anodization process for aluminum is tricky as specific anodization processes produce specific surface properties, hence it is important to reproduce the anodization procedure for specific surface finishes to obtain the same surface properties. The properties of the spacecraft have been assumed from the Foresail-1 mission design document.

component	**Coat**	**Emissivity**	**Absorptivity**
solar cell	-	0.92	-
Panel substrate	Kapton	0.65	0.82
Frame	Black Anodised	0.31	0.45

Table 6: Foresail-1 Top surface thermo-optical properties.[24]

Figure 19 and Figure 21 represent the elements which have been selected to be represented in the temperature graph. Table 6 represents the assumed properties of the Foresail-1 surface.

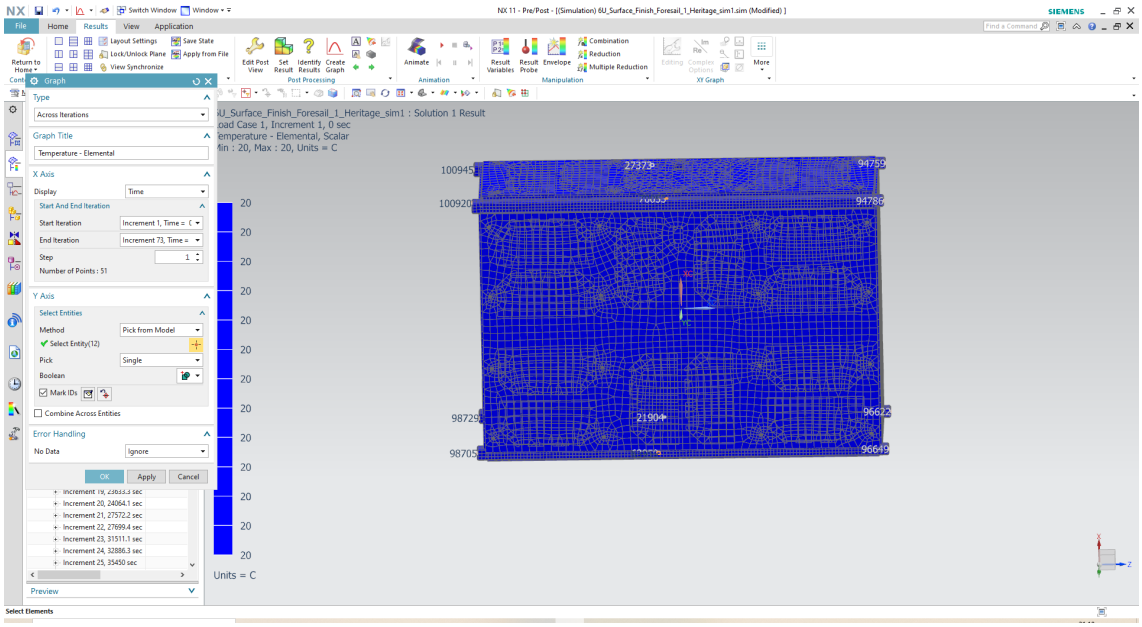

Figure 19: Elements from the structure of the Foresail-2 mission model for the thermal loading graph using Foresail-1 heritage

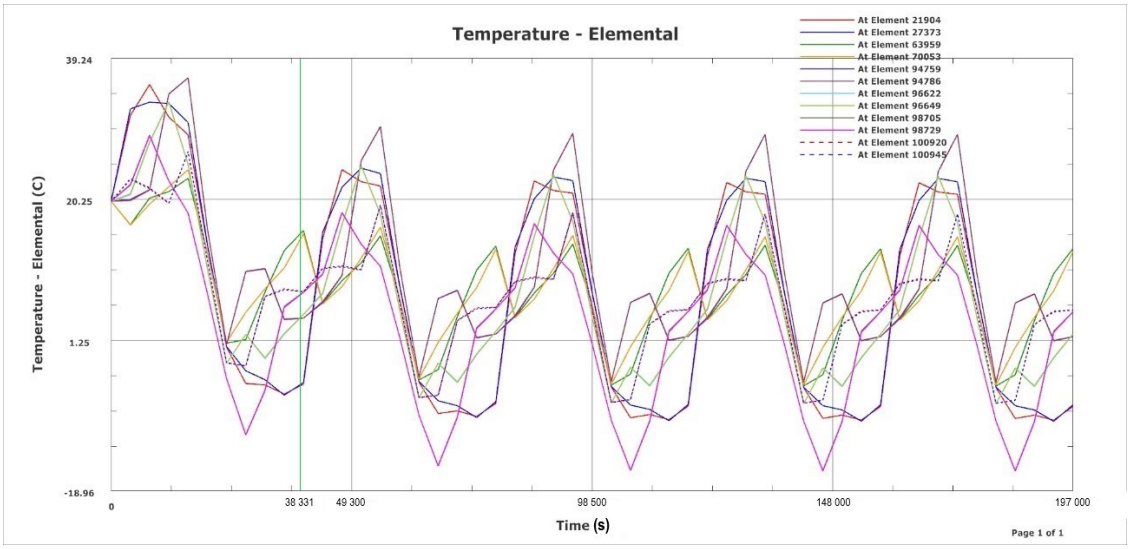

Figure 20: Foresail-2 thermal profile of the structure using foresail-1 heritage

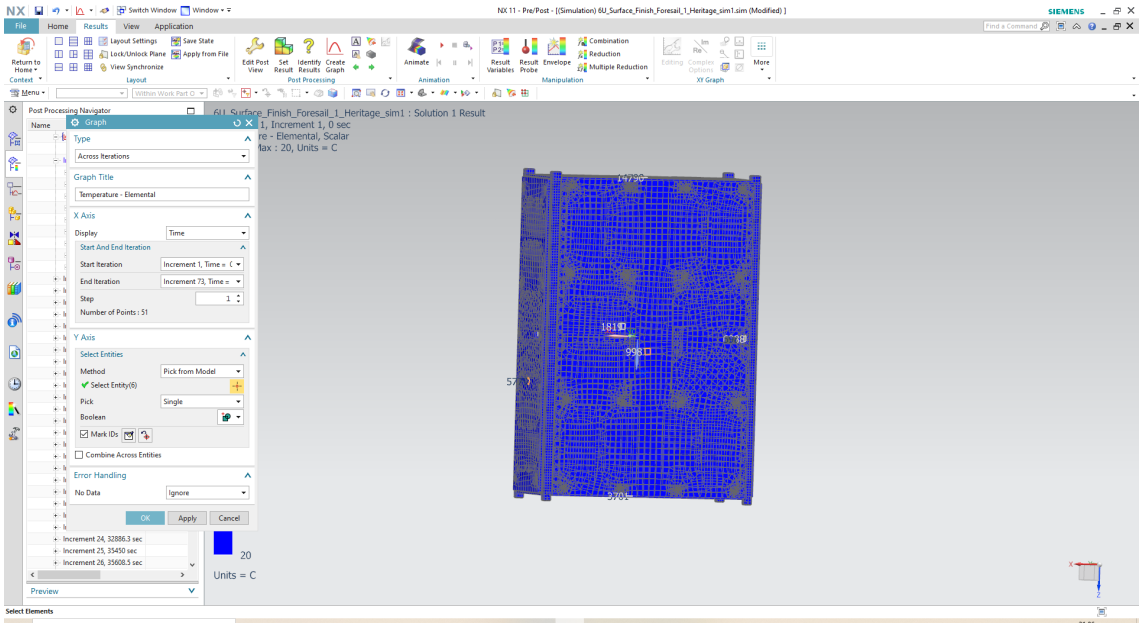

Figure 21: Foresail-2 elements for the thermal profile using Foresail-1 mission heritage

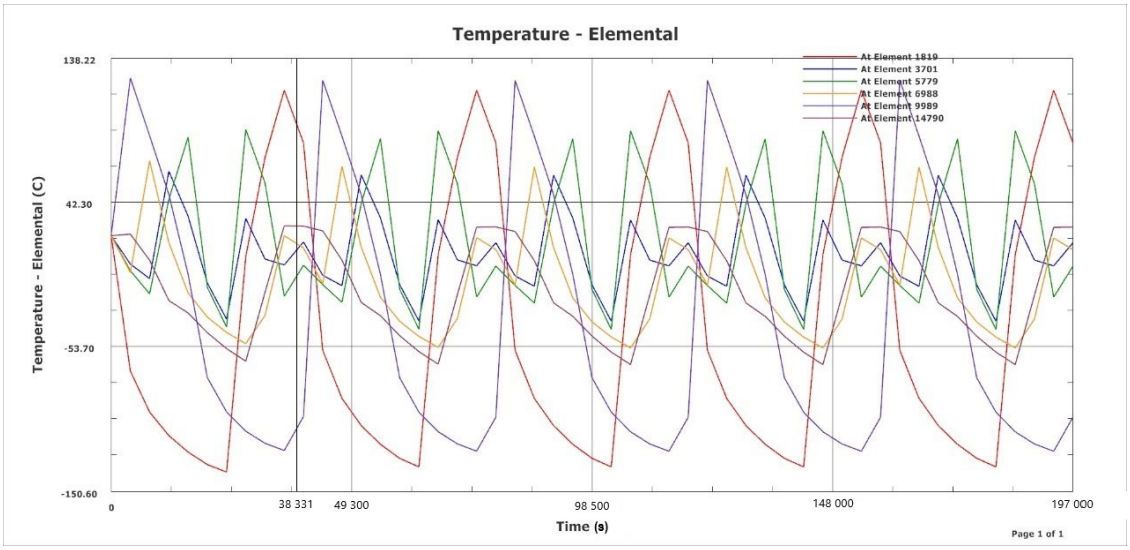

Figure 22: Foresail-2 thermal profile for the substrate using Foresail-1 heritage

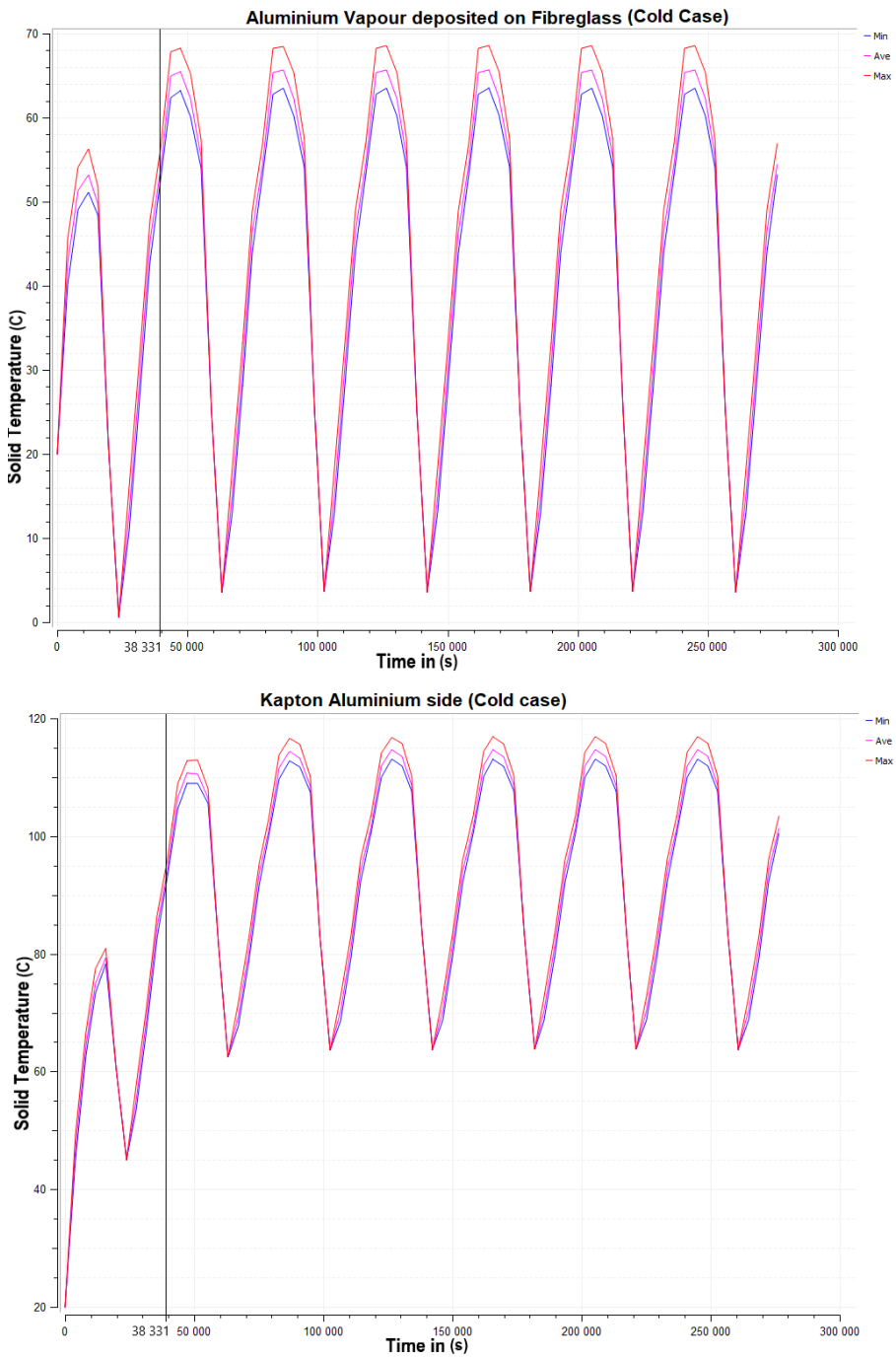

Figure 23: Temperature response of Aluminium Vapour Deposit and Al Side Kapton Tape surface finishes on a 6U CubeSat in worst case cold conditions

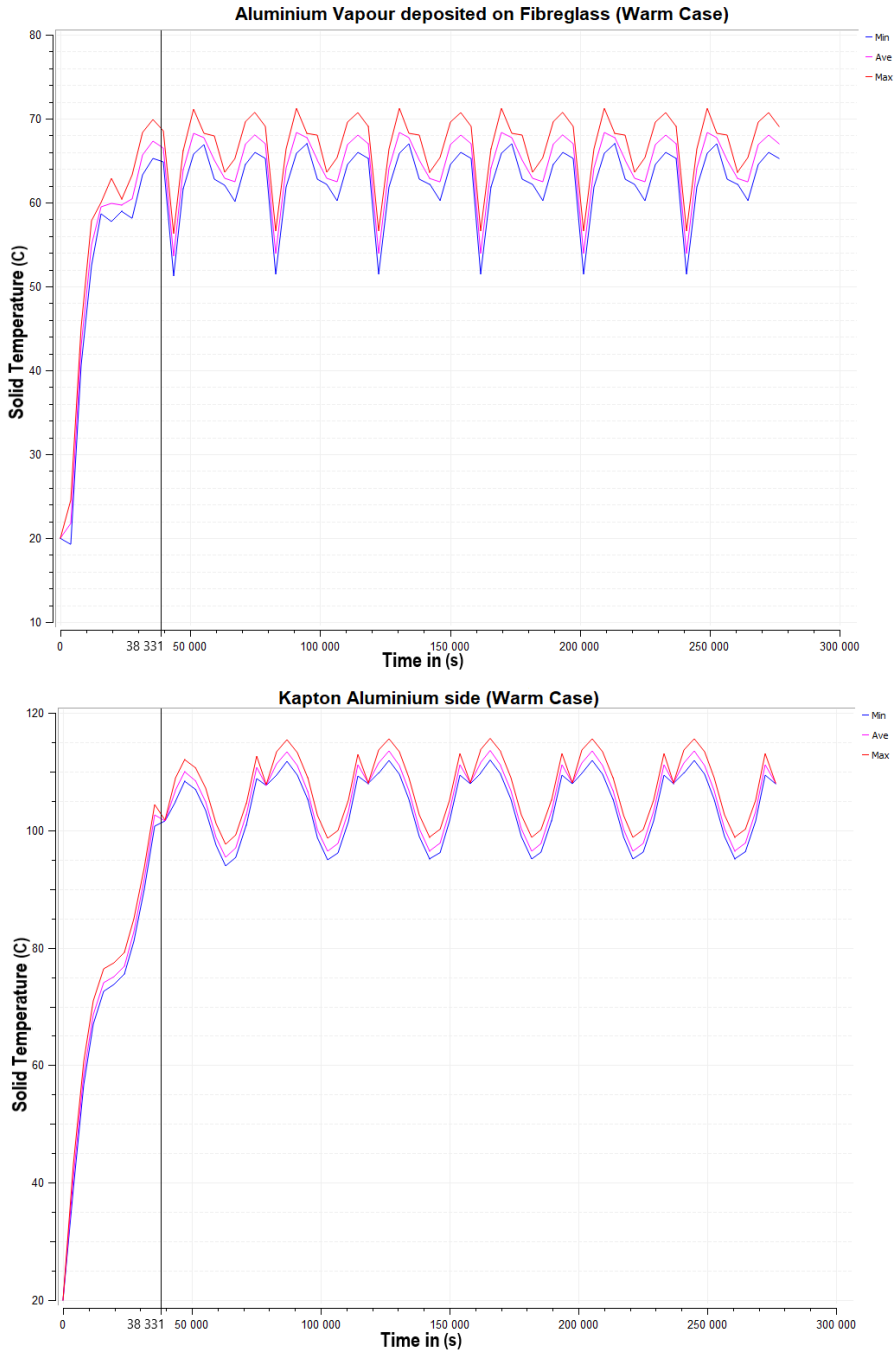

Figure 24: Temperature response of Aluminium Vapour Deposit and Al Side Kapton Tape surface finishes on a 6U CubeSat in worst case warm conditions

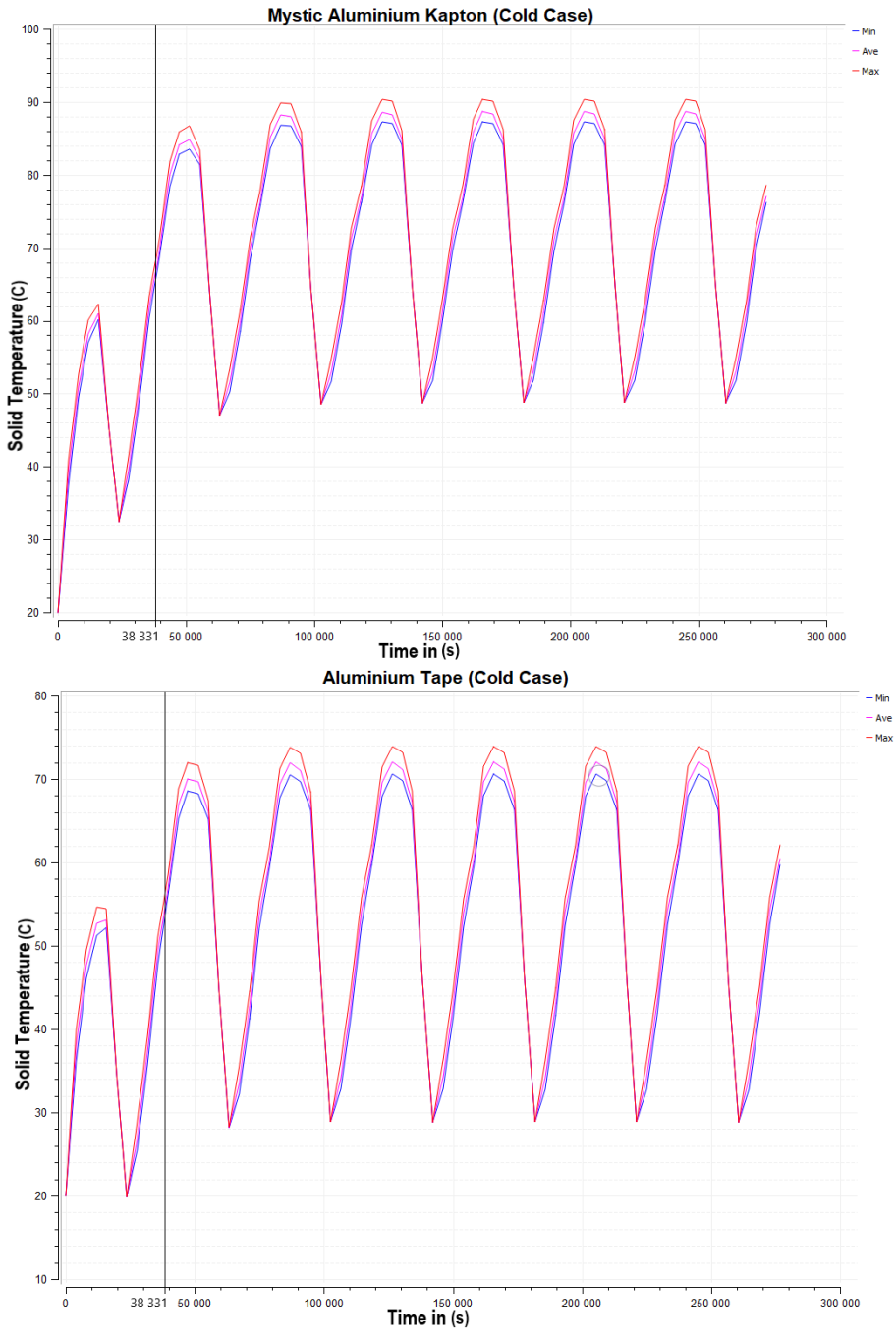

Figure 25: Temperature response of Mystic Aluminum Kapton and Aluminium Tape surface finishes on a 6U CubeSat in worst case cold conditions

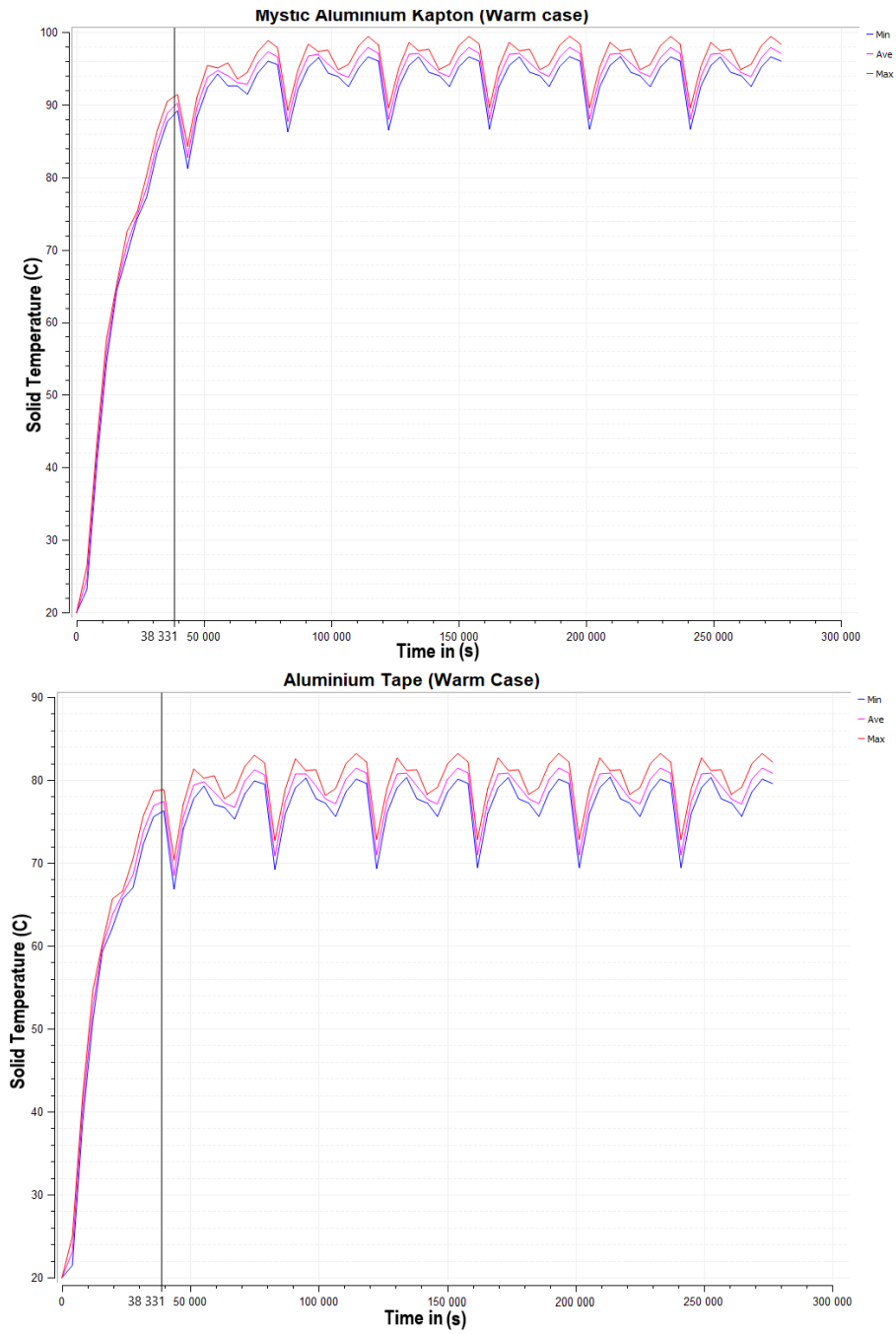

Figure 26: Temperature response of Mystic Aluminum Kapton and Aluminium Tape surface finishes on a 6U CubeSat in worst case warm conditions

Simulation for the temperature of the satellite components based on the properties assumed from the Foresail-1 mission we performed in the Siemens NX program using the space systems thermal solver. The temperature profile on the Foresail-2 mission model using the heritage from the Foresail-1 mission was obtained. The graphs for the loading on the substrate and the loading on the structure using properties from Table 6 can be observed.

The temperature profile of the elements of the spacecraft that are exposed can be observed in the Figure 20 and Figure 22. It can be seen that the solar panel needs lesser values of the absorptivity ratio so that the maximum and minimum temperatures are less extreme. The loading on the anodized structure of the spacecraft using the properties from the Foresail-1 mission appears to range between 38 to -18 degrees. The spacecraft structure reaches colder temperature in GTO.

Calculations for the surface finish on the substrate were performed on standard surface finishes as provided in [17] with properties displayed in Table 7. The response for the standard surface finishes was compared and the possible solutions were refined from it. The thermal response for maximum and minimum seasonal loading by surface finishes with most suitable thermal response can be seen in Figures 23, Figure 24, Figure 25 and Figure 26.

We observe solutions for the surface finishes on the substrate of the solar panels that will be body mounted on all sides of the spacecraft. The surface finishes were selected and refined from the list of surface finishes used in spacecraft operations. Initially, absorptive surface paints and coatings were analyzed as the spacecraft underwent severe cold loading. It was observed that this caused higher hot case loading on the spacecraft especially during the worst-case heating orbit (September solstice). Optical reflectors were rejected as the spacecraft will require to retain the heat during the eclipse phase to keep itself in the operating temperature. Trial and error method was used to select the surface finishes shown in Figure 23, Figure 24, Figure 25 and Figure 26. The above solutions do not take into consideration the area occupied by the solar cells and the heat transferred by conduction between the solar cells and the substrate. It is hence important to check the above and compare the results to select an appropriate surface finish for the solar panels once the exact details of the solar panel are obtained.

Material	**Solar α**	**IR ϵ**
Aluminium vapour deposit	0.08	0.02
Kapton Aluminium side	0.12	0.03
Mystic Aluminium Kapton	0.09	0.03
Aluminium Tape	0.10	0.04

Table 7: Properties of surface finishes used for the surface Coating loading study

5.2 Solar Panel Modelling

Body-mounted solar panels need extensive thermal analysis as general designs have subsystems mounted on the inner side of the solar panel assembly and the structure, hence having a direct conductive path from the outer surface of the solar panel to the subsystem. For the current design, we assume the components of the solar panel as documented in the Foresail-1 mission. Gallium Arsenide solar cells are mounted on the PCB. The PCB has to be standard material with FR4 regulation. The solar cell assembly is attached to the PCB using double-sided Kapton tape or space-grade Resin adhesives/ Silicone adhesives. This entire assembly is covered by a protective covering glass on the top side surface. The solar panel design will follow commonly used solar panel designs used in space applications. The entire layout of the major components used for the assembly of the solar array follows the following materials and their subsequent Thermal and/or optical properties. Figure 27 represents a simplified section of the solar panel along with the components.

The resistance diagram of the solar panel will be analyzed to find the temperature at the bottom side of the solar panel. The heat transfer vector is considered unidirectional as per the steady-state analysis. The surface heating is assumed to be uniform as the radiation from the sun is considered to be normal to the surface. It is assumed that the contacts are perfect and without irregularities hence no contact resistances are modeled into the analysis for ease of calculation. The resistance circuit diagram is solved to find the rate of heat transfer through the solar panel assembly. The properties of the materials are taken from Table 8

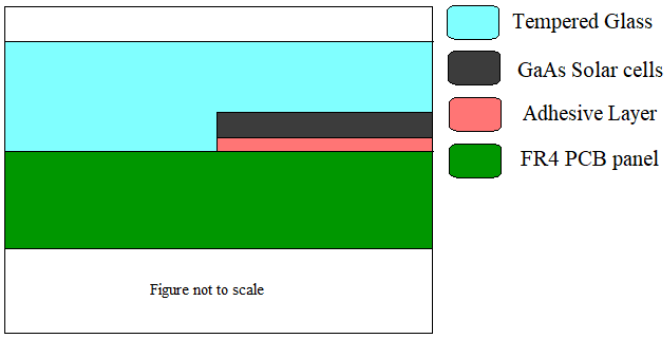

Figure 27: solar panel section

The gradient between the inside temperature and the outside temperature of the solar panel T_i and T_o respectively, divided by the total resistance of the assembly to heat flow, R_{total}, gives us the rate of heat transfer through the solar panel assembly.

$$R_s = R_1 + R_2 + R_3 \qquad \text{(K/W)}, \tag{20}$$

$$R_p = R_s + R_4 \qquad \text{(K/W)}, \tag{21}$$

$$R_{total} = R_p + R_5 \qquad \text{(K/W)}, \tag{22}$$

where R_1 is the Heat transfer resistance for tempered glass on top of the solar cells, R_2 is the heat transfer resistance of the solar cell, R_3 is the heat transfer resistance of the Adhesive layer, R_4 is the heat transfer resistance through the tempered glass in between the solar cells, R_5 is the resistance of the FR4 solar panel PCB substrate, R_s is the series reduction of the resistance circuit diagram and R_p is the parallel reduction of the resistance circuit diagram, R_{total} is the resistance of the solar panel assembly.

	Area m^2	**Conductivity** W/mK	**Thickness** m
FR4 PCB	0.06	0.4	10^{-3}
Tempered glass	0.06	0.8	$3 * 10^{-3}$
Silicone adhesive	0.035 (total)	1	$40 * 10^{-6}$
Kapton Tape	0.035 (total)	$5.24 * 10^{-3} * T^{1.02}$	$0.03 * 10^{-3}$
GaAs solar cell	0.035 (total)	52	$41.2 * 10^{-6}$

Table 8: properties of the solar panel assembly components

R_{total} is calculated to be 0.0919 K/W. The rate of heat transfer through the solar panel is found using,

$$Q = \delta T / R_{total} \qquad \text{(W)}, \tag{23}$$

where δT is the temperature difference between the top and the bottom surface.

T_o is selected at a value of 70 (Average operating temperature limit of solar panels) inside temperature T_i shall vary from $5°C$ to $40°C$ (operating limits for basic space subsystems). The rate of heat transfer shall vary depending on the difference between the outside and the inside temperature, and the rate of change in the heat transfer is plotted on MATLAB and is as shown below.

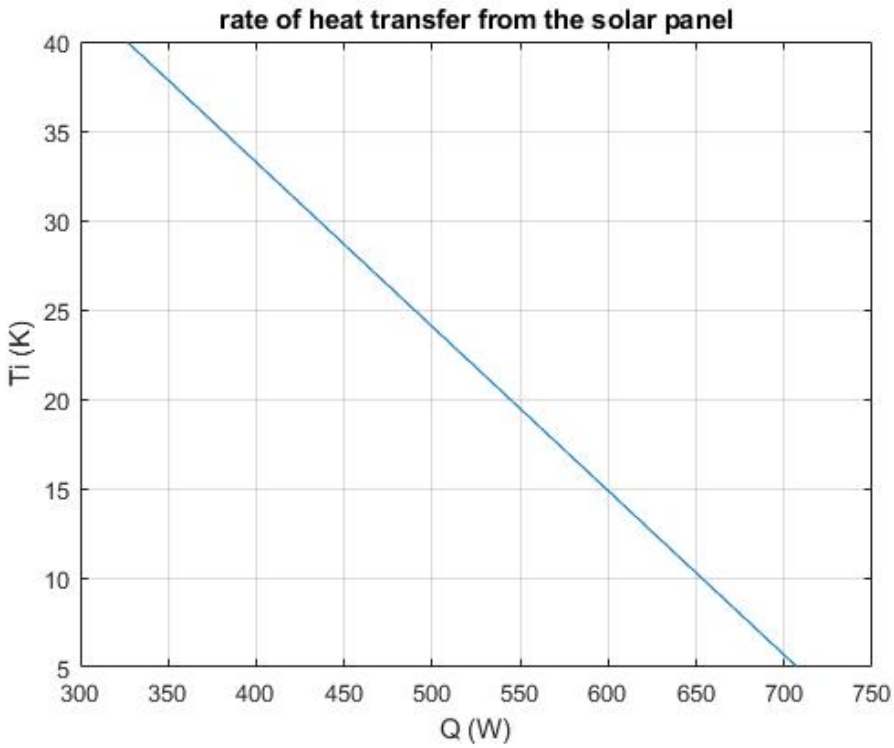

Figure 28: Heat transfer rate through the solar panel as a function of thermal gradient

From Figure 28, we can observe that as the difference between the inside and outside temperature increases, the heat transfer rate increases. The maximum difference of 65 degrees has a heat transfer rate of 707 W. Higher thermal cycling rate will cause high back and forth of heat, to and from the subsystems.

5.3 Spacecraft Internal Power

Up until now the internal heat generation of the spacecraft has not been included in the analysis of the spacecraft, but in practical applications, the internal heat will be an important aspect of the spacecraft modeling. The internal subsystem will be producing power to run operations and this power will leak as heat causing localized heating on nearby parts. Hence it is important to include the power generated by the internal subsystem so that more precise temperature graphs can be obtained.

The Foresail-2 subsystems include the three payloads, REPE, Magnetometer, and the Plasma breaking experiment. The platform subsystems include the electronics/avionics box, ADCS subsystem, and the batteries of the spacecraft which will be modeled in the simulation. The orientation of these subsystems will be dictated by the requirements set by individual subsystems, though a preliminary subsystem orientation for preliminary analysis will be assumed.

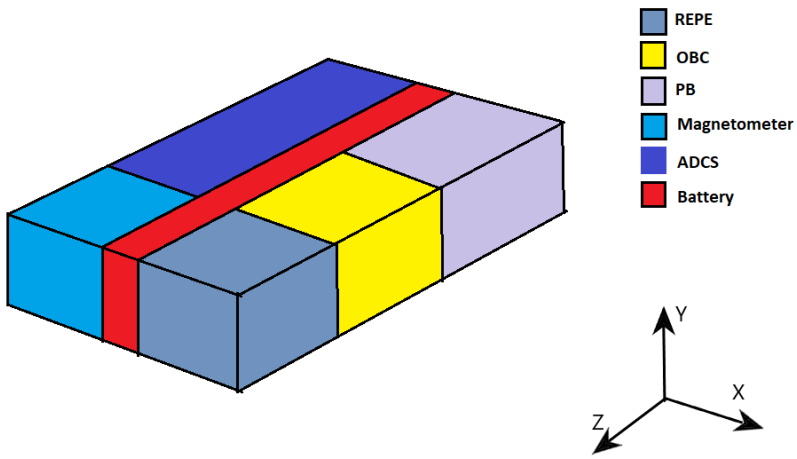

Figure 29: spacecraft subsystem positioning and orientation

The positioning of the subsystem can be observed in Figure 29. The main task of the thermal engineer is to design the spacecraft such that the subsystems of the spacecraft are maintained in the operational temperature range. To do that it is necessary to define the temperature ranges prescribed for various subsystems so that the designer is aware of what requirements are to be met. Table 9 highlights some of the general subsystems that are used for spacecraft applications and their temperature ranges. As the exact temperature ranges of the subsystems used in Foresail-2 are unavailable, we use the general temperature limits from Table 9.

Component	**operating temp** $°C$	**survival temp** $°C$
General Electronics	-10 to 45	-30 to 70
Battery	0 to 40	-5 to 60
Motors	0 to 50	-20 to 70
solar panels	-100 to 125	-120 to 150

Table 9: operational temperatures for general subsystems used in spacecraft

The power generated by the internal subsystems has to be modeled into the spacecraft heat balance equation, Equation 18, to provide a magnified view into the actual loading condition of the spacecraft. The internal heat generation of the subsystems will be provided by the subsystem designers and will be added to the power budget of the spacecraft as the power dissipated (most of the dissipated power is converted to heat). We assume the power generated by the individual components as 12 W. The analysis shall be performed with the heat dissipation being constant throughout the orbit, i.e. the subsystems will all perform at the same time throughout the orbit. This analysis will provide us with a worst-case heating condition response of the spacecraft. The subsystems will be screwed to the structure of the spacecraft and hence will be in thermal contact with the walls of the spacecraft structure. subsystems that generate excessive heat can be screwed to walls facing away from heat loads so that the heat from the subsystem will be conducted to the wall surface and radiated to space. This is trickier in rotating satellites as the spacecraft will generally be heated evenly through the orbit. The internal subsystems are generally coated with a black finish and patch heaters can be used to heat specific subsystems. Insulation can also be used between the spacecraft structure wall and the subsystem to inhibit the rate of heat transfer in cases where high thermal fluctuations are observed

5.4 Thermal Simulation Of Spacecraft

The thermal simulation of the spacecraft structure along with the internal subsystems is carried out. The simulation includes the structure of the spacecraft, the solar panel without covering the glass, and the internal subsystems. The internal subsystems produce a combined 12 W power as heat. The heat from the internal subsystems is transferred to the surroundings entirely through conduction. The heat transfer between the spacecraft and the surrounding space is through radiation from the exposed structure and the solar panel external surface. The spacecraft spins around its Y-axis, which is also in line with the spacecraft velocity vector. The orbital parameters used in previous sections shall be used. The material of the spacecraft will be as discussed in previous sections. The spacecraft structure is polished aluminum and the surface finish on the solar panels is Kapton tape. The Spacecraft structure differs as compared to the Foresail-2 structure shown in Figure 3.

The Simulation of the spacecraft loading was performed in the NX space systems solver with the space systems thermal solver. The orbital heating on the spacecraft was simulated for the defined orbit. the spacecraft model was changed and the structure of the spacecraft was changed to a simpler CubeSat structure as the time required to solve the simulation of the actual Foresail-2 model was very high. Mesh errors were also observed during the meshing of the Foresail-2 model of the spacecraft structure due to the limited operating memory of the workstation used for simulation. The main focus of the simulation is to find the response of the component loading in synergy with each other to check whether passive thermal solutions provide ample thermal control.

We can observe from the figure31 The average temperature of the satellite. We can observe that the average temperature stays in a constant range of an average of twenty degrees Celsius. The maximum and minimum temperatures in the graph are because radiation is a surface phenomenon, Hence the immediate surface facing the load will become hot though the conduction of this through the model will dissipate and spread it. Similar conditions are for the cold case. Hence we can conclude that the temperature of the spacecraft can be controlled to an operational range with passive control. It is important to simulate a better-equipped workstation. Considerable meshing defects were observed during the simulation process. Mesh defects included surfaces that could not be meshed as a solid 3D model and hence were meshed as a 2D surface. This surface will not be in proper contact with its adjoining meshes, creating high temperatures to be observed in the graph. Simplifying the model further will solve the mesh errors.

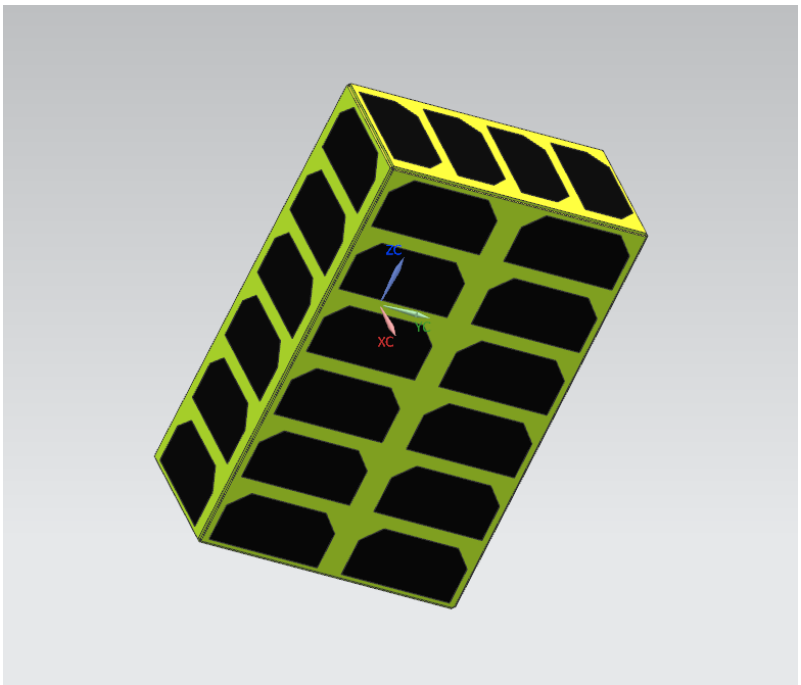

Figure 30: Assembly design For thermal analysis

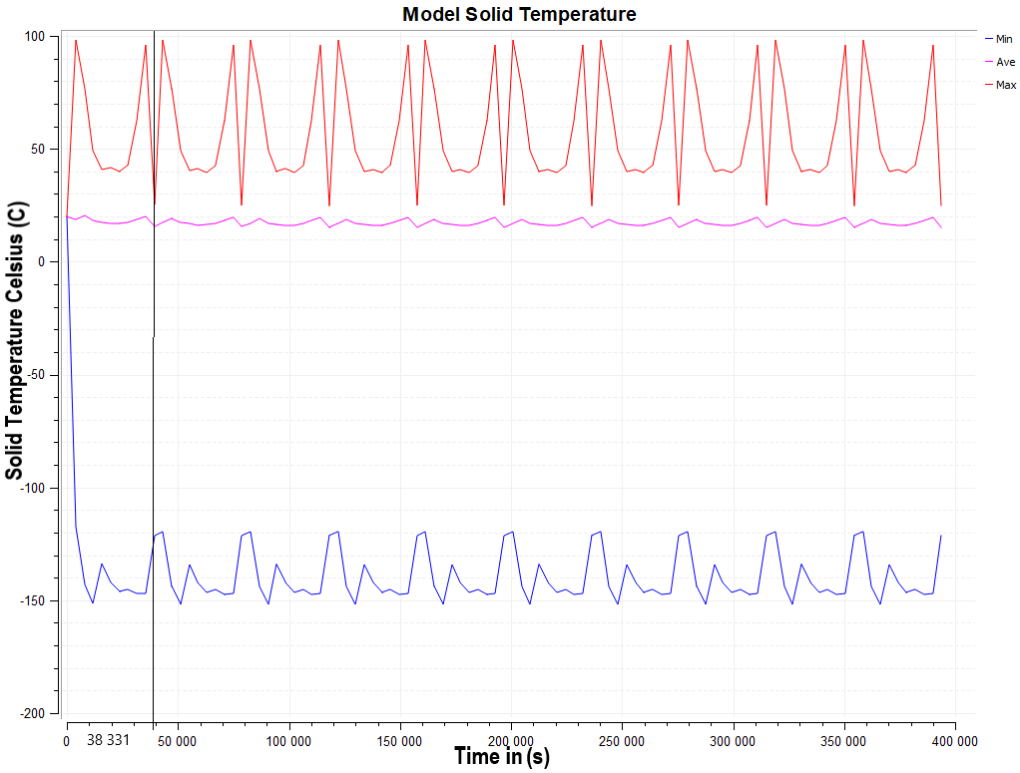

Figure 31: Average, Maximum and minimum temperature of the spacecraft for ten orbital iteration

5.5 Spacecraft Heat Transfer Model

The Heat transfer from the satellite will be three-dimensional, but we assume that the heat transfer through one of the plates of the spacecraft is one-dimensional. The heat transfer through the spacecraft sides is assumed to be one dimensional as the thickness of the spacecraft walls is small as compared to the dimension in other axes. The heat transfer through the solar panel is already calculated in previous sections and can be coupled with the structure of the satellite. This is applicable for a satellite with body-mounted solar panels. The solar panel assembly will be screwed to the satellite structure. The contact is assumed to be perfect i.e. Face defects and their impact on heat transfer are neglected.
Equation 7 is used to find the heat transfer through the plate. We assume the maximum temperature of the outer surface of the spacecraft in contact with the surrounding as T_o which is the surface temperature of the solar panel, T_i is the inside surface temperature of the spacecraft structure, T_A is the temperature of the contact between the solar panel and the spacecraft surface. R_s, R_A, and R_c are the resistances for the solar panel, the structure, and the screws respectively, where.

$$R_s = K_s * A_s/T_s \tag{24}$$

$$R_A = K_A * A_A/T_A \tag{25}$$

$$R_c = K_c * A_c/T_c \tag{26}$$

The values of R_s will be substituted into the equation directly as it has been obtained in the previous chapter. The values of K_s are not readily available as the solar panel is not one homogeneous part but an assembly. Solving the steady-state heat transfer from the solar panel will simplify the design of the steady-state heat transfer from the satellite. The heat transfer equation includes all the bodies between the internal and external surfaces that are in thermal contact.
We can observe that the resistances of the solar panel and the structure are in series hence we have

$$R_1 = R_A + R_c \tag{27}$$

R_1 is the resistance diagram simplification of the resistances in series. Similarly, we observe that the screw resistance is in parallel to 27,

$$R_{tot}{}^{-1} = R_c{}^{-1} + R_1{}^{-1} \tag{28}$$

We can find the rate of heat transfer through one of the walls of the solar panel as,

$$Q_{panel} = T_o - T_i/R_{tot} \tag{29}$$

We can find the heat transfer rate through all the sides of the spacecraft. The equation of heat transfer from the satellite is,

$$Q_{tot} = Q_x + + Q_x - + Q_y + + Q_y - + Q_z + + Q_z - \tag{30}$$

Q_x, Q_y, and Q_z denote the heat transfer through the spacecraft walls perpendicular to the principal axes of the spacecraft. T_o will vary for all the surfaces and depends

on the loading of the satellite. T_i will be common throughout the equation as the internal environment will be controlled throughout. Specific designs could have specific T_i temperatures. The area and thickness of the components of the spacecraft walls may vary and needs to be accounted for. In the equation, the area is the sum of all the areas responsible for the heat transfer of a particular material at a temperature surface. Q may be positive or negative depending on whether the spacecraft wall is losing or gaining heat. It is important to maintain the notation throughout the calculations.

It is important to model the internal temperature of the spacecraft. The internal temperature refers to the temperature of the inside walls due to the subsystem operations. Internal heat transfer modeling is more complicated as general assumptions cannot be made. The basics of the modeling process will be touched upon. The heat transfer between the internal subsystems are of two types mainly, conduction and radiation. The heat transfer solutions of internal subsystems can be performed by applying heat balance to it after identifying its thermal contacts. For the heat balance of the spacecraft, the sum of all the internal heat generation can be assumed.

Individual solutions for the internal modeling help us find and solve problems in a localized control environment, it helps us to narrow down on individual subsystems and solve the loading on them. With these equations, we can find the rate of heat transfer from the spacecraft, the time required for the spacecraft components to reach a particular temperature, or the temperature gain or loss from the spacecraft in a given time. This can be solved for the maxima and minima loading conditions to get a general solution that will be applicable through the obit of the spacecraft.

5.6 Surface Degradation

The surface of the spacecraft is subject to an extreme space environment. This causes the surface to degrade and change its properties over time. It is important to find what causes these changes on the surface so that the mission will not be jeopardized. The surface degradation that happens gradually can be mitigated if the probability of surface degradation affecting the mission is longer than the mission lifetime. The surface degradation effect can also be mitigated using specific protective coverings.

Spacecraft surface is mainly affected by atmospheric effects and can be broken down into specific effects. The main factor affecting spacecraft surfaces is vacuum UV. Ultraviolet light is emitted by the sun and is bombarded on earth. Vacuum Ultraviolet radiation is UV below 200 nm which is absorbed by particles in the atmosphere. This VUV is highly harmful to polymers and other chain compounds. VUV causes the chain links to break or causes larger chain compounds to form which causes discoloration and as a result increases the absorbtivity of the material.

Atomic oxygen penetrates the compound and causes erosion on the surface of the compound. This causes the material to get exhausted and lose its physical properties as a result. Atomic oxygen affects polymers and other similar compounds.

High altitude orbits also have to deal with high energetic particles, which cause similar reactions causing the formation of long-chain polymeric compounds with higher absorptance. Energetic particles along with VUV cause maximum damage to the spacecraft surface and have to be protected against. Other causes of surface degradation include micrometeorite and debris impact. The thermal design of the spacecraft can do little to avoid the damage caused by the impact of space debris or micrometeorites.

The expected mission duration of the Foresail-2 mission is six months. This relatively lower mission period means that the surface degradation of the surface finishes used in the Foresail-2 mission will be low. The degradation mechanism has been observed by comparing missions that were retrieved and studied and also ground experiments. while the exact mechanism of surface degradation is not well understood as the ground conditions cannot simulate exact space conditions. But using the experiments that have competed for their missions and been retrieved, and studying the surface degradation on them we can assume the general degradation graphs for commonly used space surface finishes [17].

6 Conclusion

The environmental interaction of a 6U spacecraft in an HEO orbit was performed. The HEO orbit imposes greater cold loading on the spacecraft owing to the long periods of the spacecraft under eclipse. The spacecraft will face maximum cold and hot loading during the march and September equinoxes respectively for the assumed orbital parameters. This will change depending on the orbital parameter but does depict the absolute worst-case loading. The black body radiation analysis was performed and the loading trends were analyzed, it is observed that the spacecraft will undergo severe thermal cycling while traversing through the eclipse condition, there will be significant heating from the sun until before and after the spacecraft travels under eclipse. The Longer eclipse periods of the HEO orbit cause long phases of heat loss. In a Geocentric orbit, the spacecraft will be affected by the solar, reflected solar, and IR radiation from the Earth. These are the primary causes of heat in the spacecraft along with the heat dissipated as waste heat from the internal subsystem. The influences of the loads on the spacecraft and their loading patterns were studied to assist in the process of choosing the orbit of the spacecraft. The radiation can be assumed to be a flux from the sun owing to the magnitude of the incoming radiation, The radiation intensity observed by the spacecraft for the Albedo radiation and the Earth IR radiation is dependent on the height of the spacecraft. Various other factors play into the radiation from Albedo and IR radiation such as local surface condition, surface covering, and surface visibility. The inclination of the orbit of the spacecraft causes variations in the loading on the spacecraft. As the Orbital inclination changes, the angle of incidence of the solar radiation falling on the spacecraft increases. It was observed, considering the inclination of the Earth, that maximum solar intensity is observed when the β angle of the spacecraft is minimum. This is also highly reliant on the spacecraft orbital parameters and the study made is based on the stated assumptions. The rotation of the satellite causes uniform heating of the satellite walls, which will otherwise be limited to walls that will fall under solar radiation during spacecraft orbit. It is observed that the spacecraft loading will be influenced by the rate of rotation of the satellite. Lower rates will cause higher heat transfer into the satellite and higher time to lose the same when the sides face the space environment, higher rates will restrict the time required for heat transfer to and from the satellite.

The observations made in the environmental study were used to propose possible solutions that can be incorporated into systems having similar mission objectives. A thermal engineer aims to maintain the temperature in the spacecraft under safe ranges and to have a thermal design that doesn't impose on the budget of the spacecraft. Hence, thermal designers try to make design solutions that will rely mainly on passive solutions. Passive solutions include surface finishes and coating on the spacecraft surface that will manipulate the thermo-optical properties of the spacecraft to better suit the thermal requirements. Among the various surface finishes Aluminized Kapton tape and aluminum tapes cause the most favorable loading conditions. The assumption was made for the heat dissipated by the internal subsystem and was modeled into the thermal analysis of the system using NX space systems thermal software solver environment. The loading on the spacecraft was in the temperature range under the operational range of electronics. The heat transfer calculation of a spacecraft has been modeled, this can be used to calculate the rate of heat transfer to and from the spacecraft if the internal and external heat transfer is known. From the spacecraft heat balance equation, the rate of heat transfer can be used to find one of the surface temperatures if the other is known. It is possible to use passive solutions to combat the thermal loading of the spacecraft, though it is highly dependent on the operation of the internal subsystems and the specific mission conditions of the spacecraft like the orientation, rate of rotation, and assembly of the spacecraft. The surface of the spacecraft is subject to deterioration based on its interaction with the space environment. This generally results in an increase in the solar absorptivity of the surface due to the creation of spots where the chemical properties of the surface have been changed. This mainly affects long-chain compounds such as polymers causing them to form smaller chain compounds or larger chain compounds causing discoloration spots. These spots have increased absorption. In an HEO orbit, the spacecraft is under the influence of all major surface degradation modes and hence steps need to be taken to combat such effect.

The thermal design of the spacecraft depends on specific requirements imposed on the design engineer depending on the conditions in and around the spacecraft during its operation. Hence it is difficult to suggest robust designs which can apply to all spacecraft in a similar orbit. Design changes like the inclination of the satellite orbit, the altitude of the satellite, and the orientation of the satellite cause changes in the satellite's interaction with its environment. The internal heating of the spacecraft also plays an important role in the heat balance of the spacecraft and invariably in the average temperature of the spacecraft. Yet the study can be used as a foundation, from where the design can be filtered and reworked to form an efficient thermal design.

References

[1] Larson, Wiley J., James R. Wertz; Space Mission Design and Analysis, 2nd Edition; *Published jointly by Microcosm, Inc. (Torrance, CA) and Kluwer Academic Publishers (Dordrecht/Boston/London)* 1991.

[2] Vallado, David A.; Fundamentals of Astrodynamics and Applications; *Hawthorne, CA: Microcosm Press. p. 31.* 2007.

[3] Fortescue, P.W.; Mottershead, L.J.; Swinerd, G.; Stark, J.P.W.; Spacecraft Systems Engineering; *John Wiley and Sons. ISBN 0-471-61951-5* 2003.

[4] Victoria Advocate; 'Doughnuts' of radiation ring earth in space; *(Texas). Associated Press. December 28, 1958. p. 1A*

[5] Zell, Holly; Van Allen Probes Spot an Impenetrable Barrier in Space; *NASA/Goddard Space Flight (February 12, 2015)*

[6] Timo Wekerle, José Bezerra Pessoa Filho, Luís Eduardo Vergueiro Loures da Costa, Luís Gonzaga Trabasso; Status and Trends of Smallsats and Their Launch Vehicles — An Up-to-date Review; *J. Aerosp. Technol. Manag. vol.9 no.3 São José dos Campos July/Sept. 2017*

[7] Nanosats Database; *https://www.nanosats.eu/*

[8] Aalto University Website; *https://www.aalto.fi/en/spacecraft/aalto-1-the-finnish-student-satellite-project (02-02-2021)*

[9] Aalto University Website; *https://www.aalto.fi/en/spacecraft/foresail-1 (02-02-2021)*

[10] West East Space; *https://westeastspace.com/encyclopedia/geostationary-transfer-orbit/ (02-02-2021)*

[11] Osama Khurshid, Tuomas Tikka, Jaan Praks, and Martti Hallikainen; Accommodating the plasma brake experiment on-board the Aalto-1 satellite; *Proceedings of the Estonian Academy of Sciences, 2014, 63, 2S, 258–266 doi: 10.3176/proc.2014.2S.07*

[12] Stirone, Shannon; Space Is Very Big. Some of Its New Explorers Will Be Tiny. - The success of NASA's MarCO mission means that so-called CubeSats likely will travel to distant reaches of our solar system; *The New York Times. Retrieved 18 March 2019*

[13] Finnish Centre of Excellence in Research of Sustainable Space Aalto University School of Electrical Engineering "Foresail-2 Experiment Interface Document" *02-02-2021*

[14] J Meseguer, I Pérez-Grande, A Sanz-Andrés; Spacecraft Thermal Control; *Woodhead Publishing, 1518 Walnut Street, Suite 1100, Philadelphia, PA 19102–3406, USA*

[15] Jeffery John Puschell, James Richard Wertz, David F. Everett; Space mission Engineering the new SMAD; *Hawthorne, CA : Microcosm Press : Sold and distributed worldwide by Microcosm Astronautics Books, ©2011.*

[16] Alan C. Tribble; The Space Environment implications for spacecraft design; *Princeton University Press, 2003*

[17] David G. Gilmore; Spacecraft Thermal Control Handbook Volume I: Fundamental Technologies; *Aerospace Press; Second edition (31 August 2002)*

[18] Chuss, David T.; Cosmic Background Explorer; *NASA Goddard Space Flight Center, archived from the original on May 9, 2013, retrieved 2013-04-27*

[19] Yungus A. Cengel; Heat Transfer, a practical approach; *McGraw-Hill Education; 2nd edition (16 November 2002)*

[20] Electronic notes; *https://www.electronics-notes.com/articles/satellites/basic-concepts/highly-elliptical-orbit-heo.php*

[21] Kartik Praful Naik; A Thermal investigation and comparative study of the Foresail missions; *Aalto university school of electrical engineering*

[22] Mohamed Gadalla, Mehdi Ghommem, George Bourantas, and Karol Miller; Modeling and Thermal Analysis of a Moving Spacecraft Subject to Solar Radiation Effect; *https://doi.org/10.3390/pr7110807*

[23] Assal Farrahi, and Isabel Pérez Grande; Simplified Analysis of the Thermal Behavior of a Spinning Satellite flying over Sun-synchronous orbits; *Universidad Politécnica de Madrid*

[24] Guillaume LeBonhome; Foresail-2 AOCS Trade Studies and Design; *Luleå University of Technology, Department of Computer Science, Electrical and Space Engineering.2020*

[25] Nodirkhon Yusupov; Concept studies for a CubeSat mission to the Highly Ellitical Orbit; *Tallinn University of technology, Department of Electrical Power Engineering and Mechatronics*

[26] Emanuel Escobar, Marcos Diaz, Juan Cristóbal Zagal; Evolutionary design of a satellite thermal control system: Real experiments for a CubeSat mission; *490-500. doi:10.1016/j.applthermaleng.2016.03.024*

[27] IADC Space Debris Mitigation Guidelines;Inter-Agency Space DEebris Coordination Committee, *Steering Group and Working Group 4. September 2007. Region A, Low Earth Orbit (or LEO) Region – spherical region that extends from the Earth's surface up to an altitude (Z) of 2,000 km*

[28] A. Ali, H. Ali, J. Tong, M. R. Mughal and S. U. Rehman; Modular Design and Thermal Modeling Techniques for the Power Distribution Module (PDM) of a Micro Satellite; *IEEE Access, vol. 8, pp. 160723-160737, 2020, doi: 10.1109/ACCESS.2020.302085.*

[29] M. Rizwan Mughal, et.al.; Foresail 1 platform design for particle telescope and plasma brake experiment; *Proceedings of 71st International Astronautical eCongress, IAC-20,B4,6B,x57201, Oct 2020*

[30] Zainab Saleem, et.al.; Mission design and trade off analysis of attitude and orbit control system for FORESAIL-2 CubeSat; *Proceedings of 71st International Astronautical eCongress, IAC-20,B4,IP,x60913 , Oct 2020.*

[31] M. Rizwan Mughal, et.al.; Mission overview and design approach of Foresail-1 CubeSat; *11th European CubeSat Symposium, Luxemborg, 2019.*

[32] Petri Niemela, et.al.; FORESAIL-1 satellite platform and systems design; *Finnish Satellite Workshop, Jan 20 - 22, 2020, Helsinki, Finland.*

[33] Palmroth, M., Praks, J., Vainio, R., Janhunen, P., Kilpua, E. K. J., Ganushkina, N. Yu., et al.; FORESAIL-1 cubesat mission to measure radiation belt losses and demonstrate de-orbiting; *J. Geophys. Res. Space Physics, 124. https://doi.org/10.1029/2018JA026354(2019)*

[34] Iaroslav Iakubivskyi, Pekka Janhunen, Jaan Praks, , et al.; Coulomb drag propulsion experiments of ESTCube-2 and FORESAIL-1; *Acta Astronautica, 2019, , ISSN 0094-5765, https://doi.org/10.1016/j.actaastro.2019.11.030.*

[35] Dan Bhanderi, Thomas Bak, Modeling Earth Albedo for Satellites in Earth Orbit, *DOI: 10.2514/6.2005-6465.*

A Spacecraft Rotation

The loading on the satellite surface was studied using a plate rotating in a constant load environment. The changes in the loading of the satellite due to variation of the satellite rotation speeds were observed. The relationship between the inclination of the plate and the loading on the spacecraft is the cosine between the face normal and the radiation vector from the source.

The MATLAB code calculates the incoming loads on the satellite plate for predefined time intervals. The Rotational values of the satellite are used to find the orientation of the plate at a particular time interval and the resulting loading is noted, these loading for time intervals are plotted and the resultant gives us the loading profile on a plate for a time interval. The area under the curve gives us the total energy gain of the plate for the time interval. this gives us the total loading on the plate comparatively for the time intervals that were studied.

The same principle can be used for satellites. The FEM of the satellite can be put into the loading by all the sources that cause heating on the satellite. The heat sources will be at different orientations concerning the satellite at the beginning of the simulation and need to be accounted for. The loss of heat from the satellite s simple as the view of the sink space is infinitely larger than the plate dimensions. similarly, the view factor of the sun needs not to be calculated owing to the difference in dimension. A more detailed study of the modeling of the spacecraft Thermal Loading on a satellite rotating around an axis can be studied from [23] and [22].

```
%% Variable setup %%

Gs=1414;                                    % Solar radiation W/m2
a=1;                                        % Black Body absorptivity
A=1;                                        % Unit Area plate  m^2a
t=0:0.1:60;                                 %% time in seconds 0.1 s time-
                                            % step increment %%
%% Range of RPM for the plate%

RPM1 = pi/200;                             % 0.15  RPM
RPM2 = pi/170;                             % 0.176 RPM
RPM3 = pi/150;                             % 0.2   RPM
RPM4 = pi/130;                             % 0.23  RPM
RPM5 = pi/100;                             % 0.3   RPM
RPM6 = pi/70;                              % 0.43  RPM
RPM7 = pi/50;                              % 0.6   RPM
RPM8 = pi/30;                              % 0.99  RPM
RPM9 = pi/20;                              % 1.5   RPM
RPM10 = pi/10;                             % 3     RPM
RPM11 = pi/5;                              % 6     RPM
RPM12 = pi/3;                              % 10    RPM
RPM13 = pi/2;                              % 15    RPM
RPM14 = pi;                                % 30    RPM

%% Heat flow graph for unit plate %%

Q1 = Gs.*a.*A.*cos((-pi/2)+(RPM1.*t));       % Heat transfer to the plate W
Q2 = Gs.*a.*A.*cos((-pi/2)+(RPM2.*t));
Q3 = Gs.*a.*A.*cos((-pi/2)+(RPM3.*t));
Q4 = Gs.*a.*A.*cos((-pi/2)+(RPM4.*t));
Q5 = Gs.*a.*A.*cos((-pi/2)+(RPM5.*t));
Q6 = Gs.*a.*A.*cos((-pi/2)+(RPM6.*t));
Q7 = Gs.*a.*A.*cos((-pi/2)+(RPM7.*t));
Q8 = Gs.*a.*A.*cos((-pi/2)+(RPM8.*t));
Q9 = Gs.*a.*A.*cos((-pi/2)+(RPM9.*t));
Q10 = Gs.*a.*A.*cos((-pi/2)+(RPM10.*t));
Q11 = Gs.*a.*A.*cos((-pi/2)+(RPM11.*t));
Q12 = Gs.*a.*A.*cos((-pi/2)+(RPM12.*t));
Q13 = Gs.*a.*A.*cos((-pi/2)+(RPM13.*t));
Q14 = Gs.*a.*A.*cos((-pi/2)+(RPM14.*t));

%% Limits for the graphs %%

lims1 = (Q1 >= 0);                          % positive Y axis considered
lims2 = (Q2 >= 0);
lims3 = (Q3 >= 0);
lims4 = (Q4 >= 0);
lims5 = (Q5 >= 0);
lims6 = (Q6 >= 0);
lims7 = (Q7 >= 0);
lims8 = (Q8 >= 0);
lims9 = (Q9 >= 0);
lims10 = (Q10 >= 0);
lims11 = (Q11 >= 0);
lims12 = (Q12 >= 0);
```

```
lims13 = (Q13 >= 0);
lims14 = (Q14 >= 0);

%% Area under the curve %%

A1 = trapz(t(lims1),Q1(lims1));
A2 = trapz(t(lims2),Q2(lims2));
A3 = trapz(t(lims3),Q3(lims3));
A4 = trapz(t(lims4),Q4(lims4));
A5 = trapz(t(lims5),Q5(lims5));
A6 = trapz(t(lims6),Q6(lims6));
A7 = trapz(t(lims7),Q7(lims7));
A8 = trapz(t(lims8),Q8(lims8));
A9 = trapz(t(lims9),Q9(lims9));
A10 = trapz(t(lims10),Q10(lims10));
A11 = trapz(t(lims11),Q11(lims11));
A12 = trapz(t(lims12),Q12(lims12));
A13 = trapz(t(lims13),Q13(lims13));
A14 = trapz(t(lims14),Q14(lims14));

%% Plot the heat transfer %%

plot (t,Q1)
hold on
plot (t,Q2)
hold on
plot (t,Q3)
hold on
plot (t,Q4)
hold on
plot (t,Q5)
hold on
plot (t,Q6)
hold on
plot (t,Q7)
hold on
plot (t,Q8)
hold on
plot (t,Q9)
hold on
plot (t,Q10)
hold on
plot (t,Q11)
hold on
plot (t,Q12)
hold on
plot (t,Q13)
hold on
plot (t,Q14)
hold on

ylim( [0 2e3] )
xlabel ('time in seconds')
ylabel ('enegy in watts')
title ('loading on the plate for varying rotation')
```

```
legend ('Q1','Q2','Q3','Q4','Q5','Q6','Q7','Q8','Q9','Q10','Q11','Q12','Q13','Q14')
%% Bar chart of area under the curve %%

bar (RPM1,A1,0.01)
hold on
bar (RPM2,A2,0.01)
hold on
bar (RPM3,A3,0.01)
hold on
bar (RPM4,A4,0.01)
hold on
bar (RPM5,A5,0.01)
hold on
bar (RPM6,A6,0.01)
hold on
bar (RPM7,A7,0.01)
hold on
bar (RPM8,A8,0.01)
hold on
bar (RPM9,A9,0.01)
hold on
bar (RPM10,A10,0.01)
hold on
bar (RPM11,A11,0.01)
hold on
bar (RPM12,A12,0.01)
hold on
bar (RPM13,A13,0.01)
hold on
bar (RPM14,A14,0.01)
hold on


xlabel ('Rotations Per Minute')
ylabel ('enegy in joules')
title ('loading on the plate for varying rotation')
legend ('A1','A2','A3','A4','A5','A6','A7','A8','A9','A10','A11','A12','A13','A14')
```

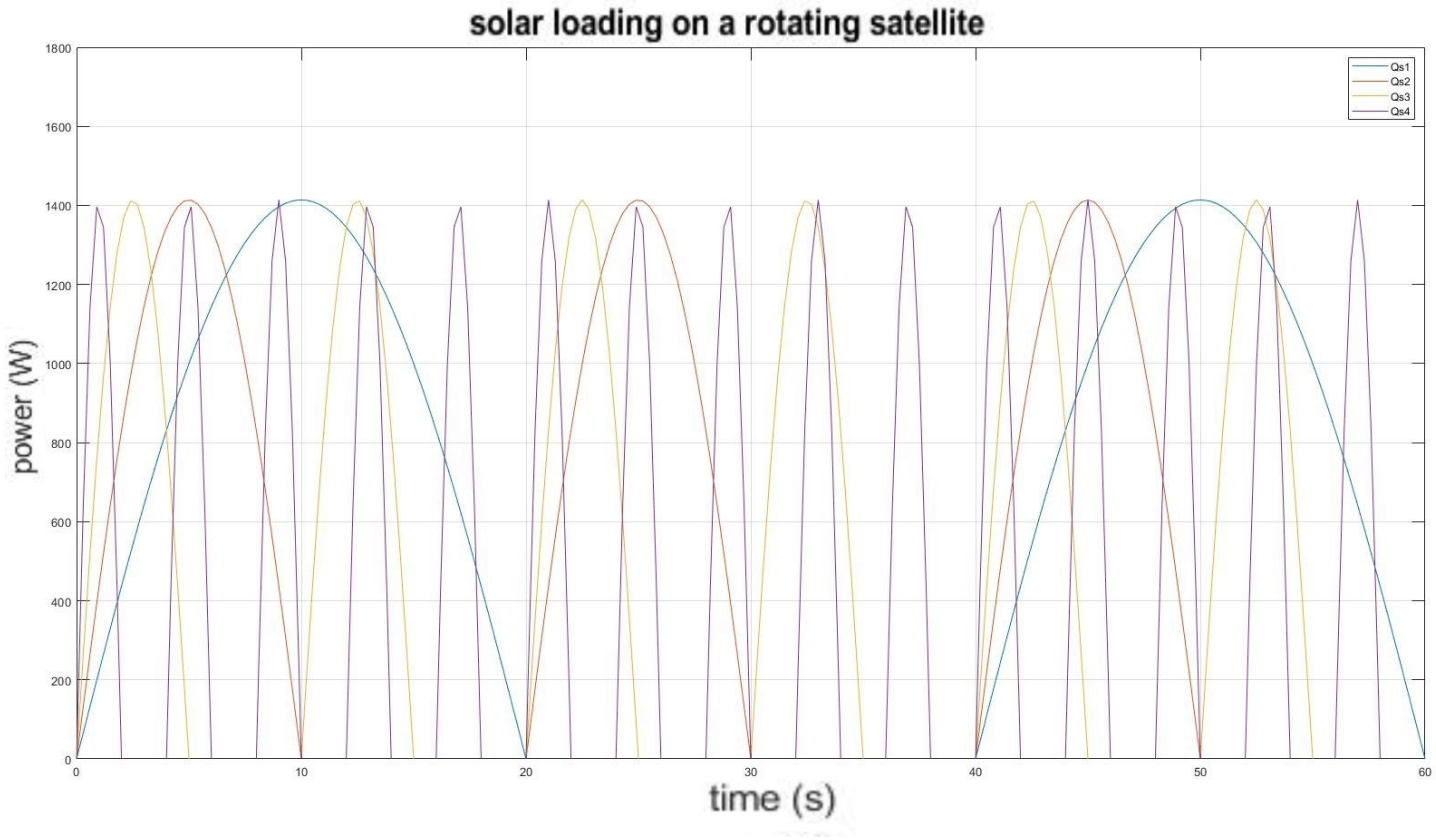

Figure A1: The heat loading on a rotating satellite for march equinox

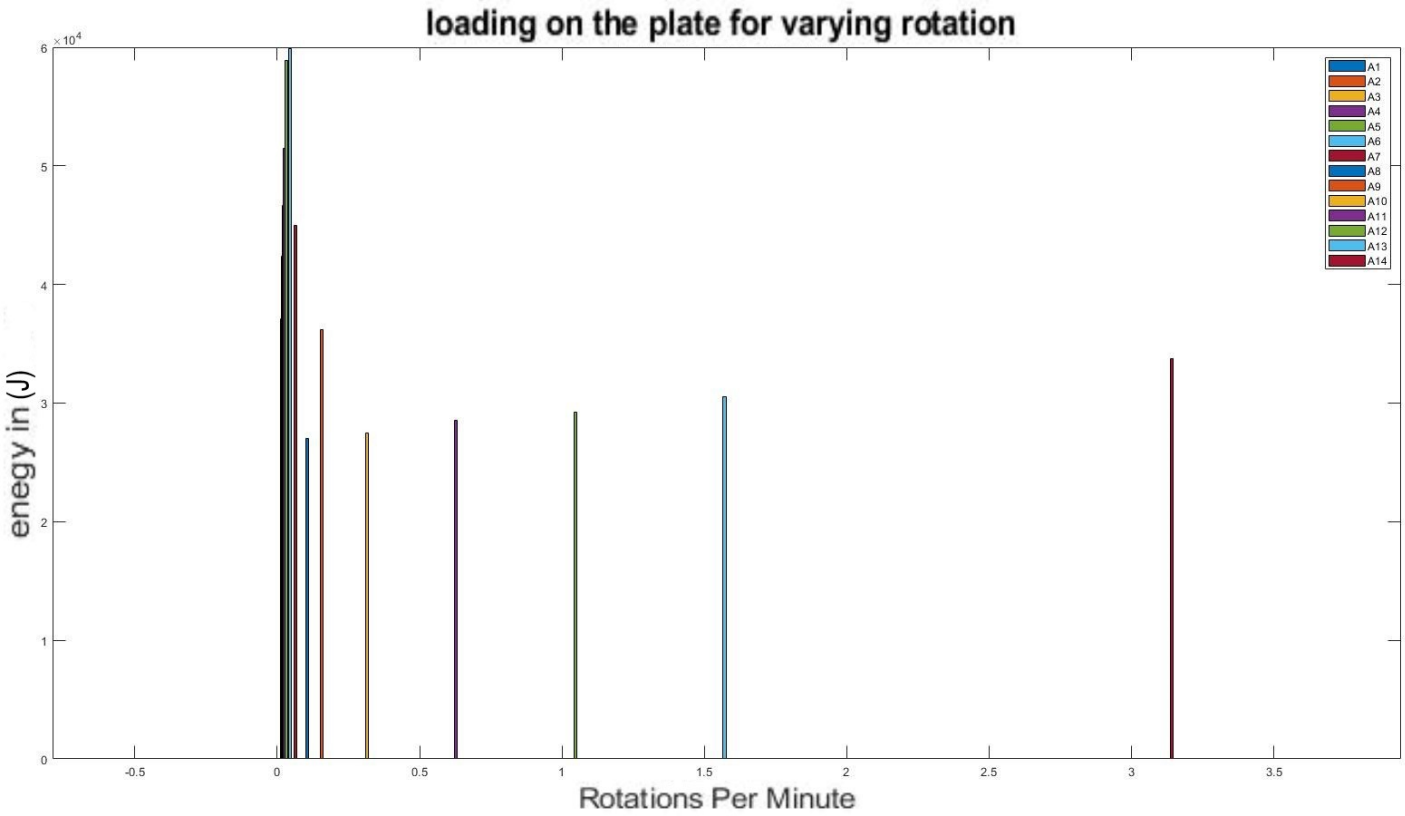

Figure A2: energy gain by unit plate for varying rotation rates